at the chromosome level in cancer cells [4]. This suggests that NHEJ helps maintain genomic integrity in mammalian cells by repairing DSBs as well as by preventing many deleterious alterations.

Acknowledgments

We thank Dr. Shunichi Takeda (Kyoto University) for providing the I-SceI expression vector pCBAISce. This study was supported by the Budget for Nuclear Research of the Ministry of Education, Culture, Sports, Science and Technology, based on screening and counseling by the Atomic Energy Commission.

REFERENCES

[1] K.K. Khanna, S.P. Jackson, DNA double-strand breaks: signaling, repair and the cancer connection, Nat. Genet. 27 (2001) 247–254.
[2] K.D. Mills, D.O. Ferguson, F.W. Alt, The role of DNA breaks in genomic instability and tumorigenesis, Immunol. Rev. 194 (2003) 77–95.
[3] D.C. van Gent, J.H. Hoeijmakers, R. Kanaar, Chromosomal stability and the DNA double-stranded break connection, Nat. Rev. Genet. 2 (2001) 196–206.
[4] J.H. Hoeijmakers, Genome maintenance mechanisms for preventing cancer, Nature 411 (2001) 366–374.
[5] E. Van Dyck, A.Z. Stasiak, A. Stasiak, S.C. West, Binding of double-strand breaks in DNA by human Rad52 protein, Nature 398 (1999) 728–731.
[6] S.P. Jackson, Sensing and repairing DNA double-strand breaks, Carcinogenesis 23 (2002) 687–696.
[7] K. Valerie, L.F. Povirk, Regulation and mechanisms of mammalian double-strand break repair, Oncogene 22 (2003) 5792–5812.
[8] P.A. Jeggo, DNA breakage and repair, Adv. Genet. 38 (1998) 185–218.
[9] E. Pastwa, J. Blasiak, Non-homologous DNA end joining, Acta Biochim. Pol. 50 (2003) 891–908.
[10] M. Honma, M. Izumi, M. Sakuraba, S. Tadokoro, H. Sakamoto, W. Wang, F. Yatagai, M. Hayashi, Deletion, rearrangement, and gene conversion; genetic consequences of chromosomal double-strand breaks in human cells, Environ. Mol. Mutagen. 42 (2003) 288–298.
[11] K. Maasho, A. Marusina, N.M. Reynolds, J.E. Coligan, F. Borrego, Efficient gene transfer into the human natural killer cell line, NKL, using the Amaxa nucleofection system, J. Immunol. Methods 284 (2004) 133–140.
[12] M. Honma, L.S. Zhang, M. Hayashi, K. Takeshita, Y. Nakagawa, N. Tanaka, T. Sofuni, Illegitimate recombination leading to allelic loss and unbalanced translocation in p53-mutated human lymphoblastoid cells, Mol. Cell Biol. 17 (1997) 4774–4781.
[13] E.E. Furth, W.G. Thilly, B.W. Penman, H.L. Liber, W.M. Rand, Quantitative assay for mutation in diploid human lymphoblasts using microtiter plates, Anal. Biochem. 110 (1981) 1–8.
[14] O. Gresch, F.B. Engel, D. Nesic, T.T. Tran, H.M. England, E.S. Hickman, I. Korner, L. Gan, S. Chen, S. Castro-Obregon, R. Hammermann, J. Wolf, H. Muller-Hartmann, M. Nix, G. Siebenkotten, G. Kraus, K. Lun, New non-viral method for gene transfer into primary cells, Methods 33 (2004) 151–163.
[15] J. Essers, H. van Steeg, J. de Wit, S.M. Swagemakers, M. Vermeij, J.H. Hoeijmakers, R. Kanaar, Homologous and non-homologous recombination differentially affect DNA damage repair in mice, EMBO J. 19 (2000) 1703–1710.
[16] S.P. Jackson, P.A. Jeggo, DNA double-strand break repair and V(D)J recombination: involvement of DNA-PK, Trends Biochem. Sci. 20 (1995) 412–415.
[17] J.M. Stark, M. Jasin, Extensive loss of heterozygosity is suppressed during homologous repair of chromosomal breaks, Mol. Cell Biol. 23 (2003) 733–743.
[18] P. Bertrand, D. Rouillard, A. Boulet, C. Levalois, T. Soussi, B.S. Lopez, Increase of spontaneous intrachromosomal homologous recombination in mammalian cells expressing a mutant p53 protein, Oncogene 14 (1997) 1117–1122.
[19] G.S. Boehden, N. Akyuz, K. Roemer, L. Wiesmuller, p53 mutated in the transactivation domain retains regulatory functions in homology-directed double-strand break repair, Oncogene 22 (2003) 4111–4117.
[20] C. Richardson, J.M. Stark, M. Ommundsen, M. Jasin, Rad51 overexpression promotes alternative double-strand break repair pathways and genome instability, Oncogene 23 (2004) 546–553.
[21] W.E. Bradley, A. Belouchi, K. Messing, The aprt heterozygote/hemizygote system for screening mutagenic agents allows detection of large deletions, Mutat. Res. 199 (1988) 131–138.
[22] H.L. Liber, D.W. Yandell, J.B. Little, A comparison of mutation induction at the tk and hprt loci in human lymphoblastoid cells; quantitative differences are due to an additional class of mutations at the autosomal tk locus, Mutat. Res. 216 (1989) 9–17.
[23] J. Dahm-Daphi, P. Hubbe, F. Horvath, R.A. El Awady, K.E. Bouffard, S.N. Powell, H. Willers, Nonhomologous end-joining of site-specific but not of radiation-induced DNA double-strand breaks is reduced in the presence of wild-type p53, Oncogene 24 (2005) 1663–1672.
[24] J. Guirouilh-Barbat, S. Huck, P. Bertrand, L. Pirzio, C. Desmaze, L. Sabatier, B.S. Lopez, Impact of the KU80 pathway on NHEJ-induced genome rearrangements in mammalian cells, Mol. Cell 14 (2004) 611–623.
[25] D. van Heemst, L. Brugmans, N.S. Verkaik, D.C. van Gent, End-joining of blunt DNA double-strand breaks in mammalian fibroblasts is precise and requires DNA-PK and XRCC4, DNA Rep. (Amst.) 3 (2004) 43–50.
[26] Z.E. Karanjawala, U. Grawunder, C.L. Hsieh, M.R. Lieber, The nonhomologous DNA end joining pathway is important for chromosome stability in primary fibroblasts, Curr. Biol. 9 (1999) 1501–1504.
[27] P. Ahnesorg, P. Smith, S.P. Jackson, XLF interacts with the XRCC4-DNA ligase IV complex to promote DNA nonhomologous end-joining, Cell 124 (2006) 301–313.
[28] D. Buck, L. Malivert, R. de Chasseval, A. Barraud, M.C. Fondaneche, O. Sanal, A. Plebani, J.L. Stephan, M. Hufnagel, F. le Deist, A. Fischer, A. Durandy, J.P. de Villartay, P. Revy, Cernunnos, a novel nonhomologous end-joining factor, is mutated in human immunodeficiency with microcephaly, Cell 124 (2006) 287–299.
[29] S. Burma, D.J. Chen, Role of DNA-PK in the cellular response to DNA double-strand breaks, DNA Rep. (Amst.) 3 (2004) 909–918.
[30] Z.E. Karanjawala, N. Adachi, R.A. Irvine, E.K. Oh, D. Shibata, K. Schwarz, C.L. Hsieh, M.R. Lieber, The embryonic lethality in DNA ligase IV-deficient mice is rescued by deletion of Ku: implications for unifying the heterogeneous phenotypes of NHEJ mutants, DNA Rep. (Amst.) 1 (2002) 1017–1026.

Available online at www.sciencedirect.com
ScienceDirect
Mutation Research 619 (2007) 113–123
Fundamental and Molecular Mechanisms of Mutagenesis
www.elsevier.com/locate/molmut
Community address: www.elsevier.com/locate/mutres

Potassium bromate treatment predominantly causes large deletions, but not GC > TA transversion in human cells

Yang Luan [a,b,c], Takayoshi Suzuki [a], Rajaguru Palanisamy [a,d], Yoshio Takashima [b], Hiroko Sakamoto [b], Mayumi Sakuraba [b], Tomoko Koizumi [b], Mika Saito [b,e], Hiroshi Matsufuji [e], Kazuo Yamagata [e], Teruhide Yamaguchi [a], Makoto Hayashi [b], Masamitsu Honma [b,*]

[a] *Division of Cellular and Gene Therapy Products, National Institute of Health Sciences, 1-18-1 Kamiyoga, Setagaya-ku, Tokyo 158-8501, Japan*
[b] *Division of Genetics and Mutagenesis, National Institute of Health Sciences, 1-18-1 Kamiyoga, Setagaya-ku, Tokyo 158-8501, Japan*
[c] *Center for Drug Safety Evaluation, Shanghai Institute of Materia Medica, Chinese Academy of Sciences, 294 Tai-Yuan Road, Shanghai 200031, China*
[d] *Department of Biotechnology, School of Engineering and Technology, Bharathidasan University, Palkalaiperur, Tiruchirappalli 620024, India*
[e] *Department of Food Science and Technology, College of Bioresource Sciences, Nihon University, 1866 Kameino, Fujisawa-shi, Kanagawa 252-8510, Japan*

Received 21 October 2006; received in revised form 24 February 2007; accepted 28 February 2007
Available online 4 March 2007

Abstract

Potassium bromate ($KBrO_3$) is strongly carcinogenic in rodents and mutagenic in bacteria and mammalian cells in vitro. The proposed genotoxic mechanism for $KBrO_3$ is oxidative DNA damage. $KBrO_3$ can generate high yields of 8-hydroxydeoxyguanosine (8OHdG) DNA adducts, which cause GC > TA transversions in cell-free systems. In this study, we investigated the in vitro genotoxicity of $KBrO_3$ in human lymphoblastoid TK6 cells using the comet (COM) assay, the micronucleus (MN) test, and the thymidine kinase (*TK*) gene mutation assay. After a 4 h treatment, the alkaline and neutral COM assay demonstrated that $KBrO_3$ directly yielded DNA damages including DNA double strand breaks (DSBs). $KBrO_3$ also induced MN and *TK* mutations concentration-dependently. At the highest concentration (5 mM), $KBrO_3$ induced MN and *TK* mutation frequencies that were over 30 times the background level. Molecular analysis revealed that 90% of the induced mutations were large deletions that involved loss of heterozygosity (LOH) at the *TK* locus. Ionizing-irradiation exhibited similar mutational spectrum in our system. These results indicate that the major genotoxicity of $KBrO_3$ may be due to DSBs that lead to large deletions rather than to 8OHdG adducts that lead to GC > TA transversions, as is commonly believed. To better understand the genotoxic mechanism of $KBrO_3$, we analyzed gene expression profiles of TK6 cells using Affymetrix Genechip. Some genes involved in stress, apoptosis, and DNA repair were up-regulated by the treatment of $KBrO_3$. However, we could not observe the similarity of gene expression profile in the treatment of $KBrO_3$ to ionizing-irradiation as well as oxidative damage inducers.

Keywords: Potassium bromate ($KBrO_3$); *TK*-mutation; Loss of heterozygosity (LOH); 8-Hydroxydeoxyguanosine (8OHdG); Gene expression profile

* Corresponding author. Tel.: +81 3 3700 1141x435; fax: +81 3 3700 2348.
E-mail address: honma@nihs.go.jp (M. Honma).

0027-5107/$ – see front matter © 2007 Elsevier B.V. All rights reserved.
doi:10.1016/j.mrfmmm.2007.02.029

1. Introduction

Potassium bromate ($KBrO_3$) is used as in bread making a flour improver and in the production of fish-pastes. The EU countries now prohibit its use as a food additive because of its carcinogenicity. Japan and the USA, however, permit its use in bread making on the condition that it never remains in the final product. $KBrO_3$ causes tumors, especially in kidney, in rats, and mice after long-term oral administration in drinking water [1–3]. $KBrO_3$ is also genotoxic. It is positive in in vitro genotoxicity tests – including the bacterial reverse mutation assay [1], the chromosomal aberration test conducted in Chinese hamster cells [4], and the mouse lymphoma assay [5] – and in vivo in the micronucleus test (MN) [6,7].

It has been proposed that $KBrO_3$ induces tumors through the production of oxidative damage to DNA. Oxidative DNA damage can cause mutations that contribute to the activation of oncogenes and/or the inactivation of tumor suppressor genes, thereby leading to tumorigenesis [8,9]. 8-Hydroxydeoxyguanosine (8OHdG) is the main form of oxidative DNA damage induced by $KBrO_3$ [10]. It primarily causes GC > TA transversions (as a result of the pairing of 8OHdG with A) and is believed to be responsible for mutagenesis, carcinogenesis, and aging [11,12]. $KBrO_3$ increases 8OHdG DNA adducts in vivo and in vitro [13–15]. However, $KBrO_3$ induces mutations weakly in microbial mutation assays and the *Hprt* mutation assay in mammalian cells, while it induces chromosome aberrations strongly both in vivo and in vitro [1,16,17]. These findings raise the question of whether 8OHdG is required for the mutagenic process involved in $KBrO_3$-induced carcinogenesis.

In the present study, we examined the genotoxic properties of $KBrO_3$ using the comet assay (COM), the MN test, and thymidine kinase (*TK*) gene mutation assays in human lymphoblastoid TK6 cells [18]. Unlike the X-linked hemizygous *HPRT* gene mutation assay, the *TK* mutation assay can detect not only point mutations, but also large scale chromosomal deletions, recombinations, and aneuploidy [19–21]. Most of the genetic changes observed in *TK* mutants occur in human tumors and are presumed relevant to carcinogenesis. We analyzed the *TK* mutants induced by $KBrO_3$ at the molecular level and investigated what kind of mutation predominated. We also profiled global gene expression in TK6 cell exposed to $KBrO_3$ using Affymetrix GeneChip® Expression analysis to understand the genotoxic mechanism of $KBrO_3$.

2. Materials and methods

2.1. Cell culture, chemicals, and treatment

The TK6 human lymphoblastoid cell line has been described previously [22]. Cells were maintained in RPMI 1640 medium (Gibco-BRL, Life Technology Inc., Grand Island, NY) supplemented with 10% heat-inactivated horse serum (JR Biosciences, Lenexa, KS), 200 μg/ml sodium pyruvate, 100 U/ml penicillin, and 100 μg/ml streptomycin. The cultures were incubated at 37 °C in a 5% CO_2 atmosphere with 100% humidity. $KBrO_3$ (CAS No.7758-01-2) was purchased from Wako Pure Chemical Co. (Tokyo) and dissolved in RPMI medium just before use.

We prepared 20 ml aliquots of cell suspension at a concentration of 5.0×10^5 cells/ml in 50 ml polystyrene tubes. Different concentrations of $KBrO_3$ were added to the tubes, which were then placed on a platform shaker and incubated at 37 °C for 4 h with gentle shaking. At the end of the treatment period, the cell cultures were centrifuged, washed once, and re-suspended in fresh medium. We cultured them in new flasks for the MN assay and *TK* gene mutation assay, or diluted them for plating for survival estimates.

2.2. Genotoxicity assays

After treating cells with $KBrO_3$, we prepared slides for conducting the alkaline and neutral COM assay. The alkaline COM assay was performed as previously reported [23]. For the neutral COM assay, the slide was electrophoresed with chilled neutral solution (pH 8) containing of 90 mM Tris, 2 mM Na_2EDTA, and 90 mM boric acid according to the method by Wada et al. [24]. The COM slides were stained with SYBER green (Molecular Probes, Eugene, OR) and observed by an Olympus model BX50 fluorescence microscope. At least 50 cells were captured by CCD camera, and tail length of the comet was measured. The relationship between $KBrO_3$ treatment and migration was statistically analyzed by the Dunnett test [25].

We prepared the MN test samples 48 h after treatment, as previously reported [23]. Briefly, approximately 10^6 cells suspended in hypotonic KCl solution were incubated for 10 min at room temperature, fixed twice with ice-cold methanol containing 25% acetic acid, then re-suspended in methanol containing 1% acetic acid. A drop of the suspension was placed on a clean glass slide and air-dried. The cells were stained with 40 μg/ml acridine orange solution and immediately observed with the aid of an Olympus model BX50 fluorescence microscope equipped with a U-MWBV band pass filter. At least 1000 intact interphase cells for each treatment were examined, and the cells containing MN were scored. The MN frequencies between non-treated and treated cells were statistically analyzed by Fisher's exact test [26].

We prepared the *TK* gene mutation assay samples 3 days after treatment. We seeded cells from each culture into 96-well plates at 40,000 cells/well in the presence of 3.0 μg/ml trifluo-

rothymidine (TFT). We also plated 1.6 cells/well without TFT to determine plating efficiency. All plates were incubated at 37 °C in a humidified atmosphere of 5% CO_2 in air. After 14 days, we scored colonies on the PE plates and the normal-growing (NG) *TK* mutants on the TFT plates, then re-fed the plates containing TFT with fresh TFT, incubated them for an additional 14 days, and scored them for slow-growing (SG) *TK* mutants. Mutation frequencies, relative survival (RS), and relative suspension growth (RSG) were calculated as previously described [23]. The data of mutant frequencies were statistically analyzed by Omori's method, which consists of a modified Dunnett's procedure for identifying clear negative, a Simpson–Margolin procedure for detecting downturn data, and a trend test to evaluate the dose-dependency [27].

2.3. LOH analysis of TK mutations by polymerase chain reaction (PCR)

To avoid analyzing identical mutants, we performed an additional *TK* mutation assay and isolated *TK* mutants from independent culture after a 4 h treatment with 2.5 mM $KBrO_3$. We confirmed the phenotype of the *TK* mutant clones by re-challenging them with TFT medium. We also determined the growth rate of the clones and confirmed whether they were NG or SG mutants.

Genomic DNA was extracted from the *TK* mutant cells and used as a template for PCR. We conducted the PCR-based LOH analysis of the human *TK* gene as described previously [28]. A set of primers was used to each amplify the parts of exons 4 and 7 of the *TK* gene that is heterozygous for frame shift mutations. A third primer set for amplifying parts of the β-globin was also used as the internal control. We applied quantitative-multiple PCR for co-amplification of the three regions. The PCR products were analyzed with an ABI310 genetic analyzer (PE Biosystems, Chiba, Japan), and were classified into "no LOH", "hemizygous (hemi-) LOH", or "homozygous (homo-) LOH". To determine the extent of the LOH, we analyzed 10 microsatellite loci on chromosome 17q by PCR-based LOH analysis [28]. The results were processed by GenoTyper™ software (PE Biosystems, Chiba, Japan) according to the manufacturer's guidelines.

2.4. Gene expression analysis

Total RNA was isolated from the TK6 cells after 4 h treatment with 2.5 mM $KBrO_3$ and was purified by RNeasy columns (Qiagen, Valencia, CA). We conducted a single cDNA synthesis, cRNA labeling, and cRNA fragmentation according to the manufacturer's recommendations (Affymetrix Inc., Santa Clara, CA) and employed Affymetrix GeneChip Expression analysis. The hybridization mixture for each sample was hybridized to an Affymetrix U133A human genome array. We processed the scanned data using Microarray Suite Software Version 5.0 (Affymetrix Inc., Santa Clara, CA) and imported the data into GeneSpring software (Silicon Genetics, Redwood City, CA). Signal intensity was normalized by per-gene and per-chip, and the ratios were calculated by normalizing $KBrO_3$ sample to the corresponding control sample. We used intensity-dependent (step-wise) selection of significant changes with higher cut-off value for lower signal intensity (1.75-, 2.0-, 2.25-, 2.5-, and 3.5-fold for genes intensity range of >1000, 500–1000, 100–500, 50–100, and 10–50, respectively), and up-regulated genes with a presence call in $KBrO_3$ sample, whereas down-regulated genes with a presence call in the control sample.

3. Results

3.1. Cytotoxicity and genotoxicity of $KBrO_3$

$KBrO_3$ exerted strong and concentration-dependent cytotoxicity in TK6 cells (Fig. 1). It induced approximately 50% cytotoxicity (51% RSG and 44% RS) at 2.5 mM. To investigate whether $KBrO_3$ directly causes DNA damage, we conducted the COM assay. Induction of COM tail after the treatment of in alkaline version was statistically significant 2.5 and 5 mM. In the neutral COM assay, the induction was observed form the lower concentration (Fig. 1). Because the neutral COM is thought to be associated with DNA double strand breaks (DSBs) [29], this result indicates that $KBrO_3$ directly causes DNA damage including DSBs. $KBrO_3$ also induced MN and *TK* mutation in a concentration-dependent manner and their inductions were statistically significant (Fig. 1). At the maximum concentration, it induced both MN and *TK* mutation frequencies about 30 times the control values. Two distinct phenotypic classes of *TK* mutants were generated: NG mutants grew at the same rate as the wild type (doubling time 13–17 h), and SG mutants grew at a slower rate (doubling time > 21 h). NG mutants result from intragenic mutations, while SG mutants result from gross changes (extending beyond the *TK* gene) [20]. $KBrO_3$ predominantly induced SG mutants (Fig. 1), implying that $KBrO_3$ treatment predominantly causes gross structural changes, but not small genetic alterations such as point mutations.

3.2. Molecular analysis of TK mutants

The *TK* mutants were randomly isolated from independent cultures treated with 2.5 mM $KBrO_3$ for 4 h. Table 1 shows the cytotoxicity (RSG), mutation frequency, and proportion of SG mutants induced by $KBrO_3$. We subjected 40 induced mutants to LOH analysis. Of those, 32 (80%) were SG mutants, which corresponded closely to the percentage of SG mutants induced in the assay (74.1%), indicating that the result of LOH analysis reflected the character of the induced

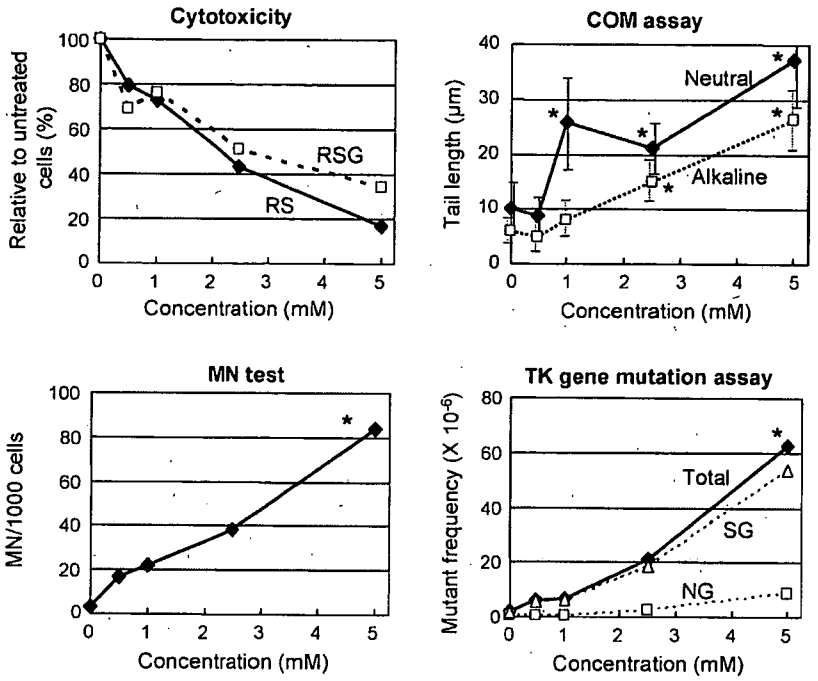

Fig. 1. Cytotoxic (relative survival, RS; relative suspension growth, RSG) and genotoxic responses (COM assay, MN test, and *TK* gene mutation assay) of TK6 cells treated with $KBrO_3$ for 4 h. Asterisk (*) statistically significant in Dunnett's test ($P < 0.05$) in COM assay, and in both pair-wise comparison and trend test ($P < 0.05$) in MN test and *TK* gene mutation assay.

mutations. Table 1 also shows the results of LOH analysis of the induced and spontaneously occurring mutants. The result of molecular analysis of spontaneous *TK* mutants was reported previously [21]. We classified the mutants into three types: non-LOH, hemizygous LOH (hemi-LOH), and homozygous LOH (homo-LOH). In general, hemi-LOH is resulted by deletion and homo-LOH is by inter-allelic homologous recombination [20]. Among the $KBrO_3$-induced mutants, 63% of NG mutants and 84% of SG mutants were hemi-LOH. In spontaneous mutants, on the other hand, majority of NG and SG mutants were non-LOH and homo-LOH, respectively. These results indicated that $KBrO_3$ predominantly induced large deletions. We previously reported the mutational spectra of *TK* mutants in TK6 cells that treated with the alkylating agent ethylmethane sulfonate (EMS), or X-irradiated [20,21]. Fig. 2 shows the comparison of the mutational spectra of spontaneous and induced *TK* mutants by EMS, X-irradiation, and $KBrO_3$. The mutation spectrum induced by $KBrO_3$ was similar to that induced by X-radiation (which also induces LOH, predominantly via deletion [21]) but not by EMS. The majority of the mutations induced by $KBrO_3$ were large deletions, but not point mutations.

Fig. 3 shows the regions of LOH and the distribution of spontaneous, X-ray-induced, and $KBrO_3$-induced

Table 1
Cytotoxic and mutational responses to $KBrO_3$, and the results of LOH analysis of normally growing (NG) and slowly growing (SG) *TK* mutants

Treatment	Cytotoxic and mutational response			LOH analysis at *TK* gene (%)			
	RSG (%)	MF ($\times 10^{-6}$)	% SG	Number	Non-LOH	Hemi-LOH	Homo-LOH
Spontaneous[a]	100	2.19	56	56			
NG mutants				19	14(74)	3(16)	2(11)
SG mutants				37	0(0)	9(24)	28(76)
$KBrO_3$ (2.5 mM)	51	29.4	74	39			
NG mutants				8	3(37)	5(63)	0(0)
SG mutants				31	1(3)	27(84)	4(13)

[a] Data from Zhan et al. [22].

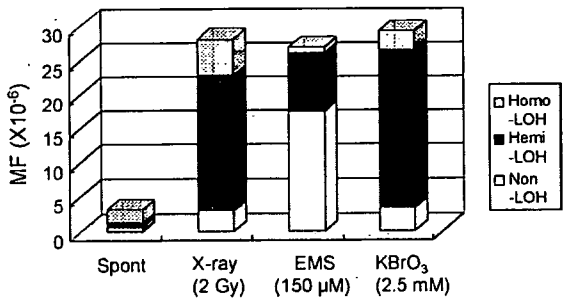

Fig. 2. *TK* mutation spectra in untreated, X-ray-treated (2 Gy), EMS-treated (150 μM, 4 h), and $KBrO_3$-treated (2.5 mM, 4 h) TK6 cells. The fraction of each mutational event was calculated by considering the ratio of NG to SG mutants and the results of molecular analysis (Table 1). The data for all but the $KBrO_3$ treatments were taken from our previous paper [20].

LOH mutants. $KBrO_3$ predominantly induced hemi-LOH, the result of large interstitial and terminal deletions, which we also frequently observed in the X-ray-induced LOH mutants. These results indicate that the genetic changes induced by $KBrO_3$ were similar to those induced by X-rays.

3.3. Gene expression analysis

Table 2 lists the genes that significantly increased expression following exposure to 2.5 mM $KBrO_3$. These genes are involved in stress response (6 genes), cell growth and DNA repair (19 genes), immune response (3 genes), apoptosis (3 genes), signal transduction (10 genes), transcription regulation (10 genes), chromosome organization (2 genes), protein modification (7 genes), energy metabolism (6 genes), lipid metabolism (2 genes), purine biosynthesis (3 genes), and unclassified functions (42 genes). Table 3 shows the genes whose expression was suppressed by the treatment. The number of up-regulated genes was greater that the number of down-regulated genes.

4. Discussion

$KBrO_3$ is a complete carcinogen, possessing both initiating and promoting activities in rodents [1]. While it shows clear positive responses in the COM assay, MN test, and chromosome aberration test using mammalian cells [4,14,17], the mutagenic potential of $KBrO_3$ in bacteria and the *Hprt* assay in Chinese hamster cells is weak or negative [1,14,17,30]. In our present study, $KBrO_3$ treatment strongly induced *TK* gene mutations. The reason we observed the induction of gene mutations and others did not is that $KBrO_3$ induces detectable mutagenecity in the *TK* gene but are only weakly mutagenic or non-mutagenic in the *Hprt* gene and in microbial assays [20]. The lower mutation frequency in the *Hprt* gene is due to the low recovery of large deletions, which are not detected because they are lethal. $KBrO_3$ is positive in mouse lymphoma cell assays that target the *Tk* gene [5]. In in vivo genotoxicity tests, $KBrO_3$ strongly induces MN in male ddY mice but is only weakly mutagenic in the *gpt* mutation assay in transgenic mice, which mainly detects point mutations and small deletions [31]. These results indicate that the property of genotoxicity

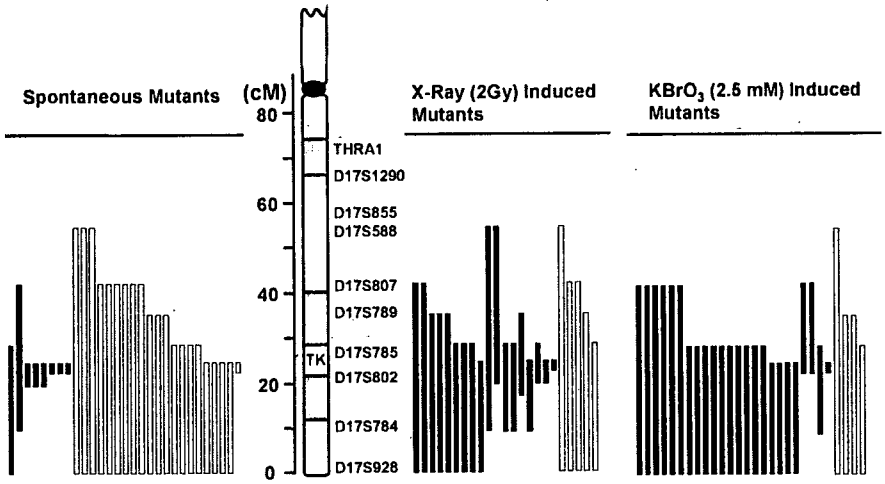

Fig. 3. The extent of LOH at the *TK* locus of TK6 cells that were untreated, X-ray-irradiated (2 Gy), or exposed to $KBrO_3$ (2.5 mM, 4 h). We examined 10 microsatellite loci on chromosome 17q that are heterozygous in TK6 cells. The human *TK* locus maps to 17q23.2. Open and closed bars represent homozygous LOH and hemizygous LOH, respectively. The length of the bar indicates the extent of the LOH. We analyzed 28 LOH mutants (4 NG and 24 SG). The data on spontaneous and X-ray-induced mutants were taken from our previous paper [20].

Table 2
Genes whose expression was up-regulated by $KBrO_3$ (2.5 mM, 4 h)

	Gene symbol	Ratio	Gene title
Stress response	CAT	2.77	Catalase
	DNAJC7	2.33	DnaJ (Hsp40) homolog, subfamily C, member 7
	FKBP5	2.87	FK506 binding protein 5
	HSPA8	3.02	Heat shock 70 kDa protein 8
	HSPCB	3.21	Heat shock 90 kDa protein 1, beta
	HSPD1	1.83	Heat shock 60 kDa protein 1
DNA repair, cell cycle, cell growth	BUB1	4.51	BUB1 budding uninhibited by benzimidazoles 1 homolog
	CCND2	5.08	Cyclin d2
	CCT2	3.33	Chaperonin containing TCP1, subunit 2 (beta)
	DKC1	2.37	Dyskeratosis congenita 1, dyskerin
	ENO1	2.10	Enolase 1 (alpha)
	HMGB1	2.16	High-mobility group box 1
	MAPRE1	2.32	Microtubule-associated protein, RP/EB family, member 1
	NME1	2.00	Non-metastatic cells 1, protein (NM23A) expressed in
	NOLC1	2.99	Nucleolar and coiled-body phosphoprotein 1
	NRAS	2.54	Neuroblastoma RAS viral (v-ras) oncogene homolog
	p21	3.22	Cyclin-dependent kinase inhibitor 1A (p21, Cip1)
	PPP2R1B	2.45	Protein phosphatase 2 (formerly 2A), regulatory subunit A (PR 65), beta isoform
	RAD21	2 34	RAD21 homolog
	RBBP4	2.00	Retinoblastoma binding protein 4
	RHOA	1.77	ras homolog gene family, member A
	SRPK1	2.75	SFRS protein kinase 1
	SSR1	2.66	Signal sequence receptor, alpha
Immune response	ARHGDIB	1.78	Rho GDP dissociation inhibitor (GDI) beta
	HLA-DRA	2.16	Major histocompatibility complex, class II, DR alpha
	IL2RG	2.43	Interleukin 2 receptor, gamma
Apoptosis	BCLAF1	6.42	BCL2-associated transcription factor 1
	FXR1	3.32	Fragile X mental retardation, autosomal homolog 1
	VDAC1	1.94	Voltage-dependent anion channel 1
Signal transduction	ANP32A	3.20	Acidic (leucine-rich) nuclear phosphoprotein 32 family, member A
	OGT	2.74	O-linked *N*-acetylglucosamine (GlcNAc) transferase
	PIP5K1A	4.25	Phosphatidylinositol-4-phosphate 5-kinase, type I, alpha
	PLEK	2.95	Pleckstrin
	PTPN11	2.61	Protein tyrosine phosphatase, non-receptor type 11
	SPTLC1	2.62	Serine palmitoyltransferase, long chain base subunit 1
	SRPR	2.52	Signal recognition particle receptor
Transcription regulation	CDC5L	4.37	CDC5 cell division cycle 5-like
	HNRPC	4.40	Heterogeneous nuclear ribonucleoprotein C (C1/C2)
	MED6	2.45	Mediator of RNA polymerase II transcription, subunit 6 homolog
	MED6	2.45	Mediator of RNA polymerase II transcription, subunit 6 homolog
	NO NO	2.68	Non-POU domain containing, octamer-binding
	POLR1C	2.67	Polymerase (RNA) I polypeptide C, 30 kDa
	PRPF4	2.51	PRP4 pre-mRNA processing factor 4 homolog
Chromosome organization	CBX5	2.68	Chromobox homolog 5 (HP1 alpha homolog, Drosophila)
Protein modification	CANX	2.56	Calnexin
	COPA	6.55	Coatomer protein complex, subunit alpha
	EIF2S3	2.40	Eukaryotic translation initiation factor 2, subunit 3 gamma
	EIF4B	2.86	Eukaryotic translation initiation factor 4B
	RANBP2	3.96	RAN binding protein 2
	SEC23IP	2.67	SEC23 interacting protein

Table 2 (*Continued*)

	Gene symbol	Ratio	Gene title
Energy pathway	AFURS1	2.83	ATPase family homolog up-regulated in senescence cells
	CYB5-M	2.54	Cytochrome *b5* outer mitochondrial membrane precursor
	TOMM22	3.07	Translocase of outer mitochondrial membrane 22 homolog
Lipid metabolism	HMGCS1	2.58	3-Hydroxy-3-methylglutaryl-Coenzyme A synthase 1
	SCD	2.56	Stearovl-CoA desaturase
Purine biosynthesis	ENTPD1	2.36	Ectonucleoside triphosphate diphosphohydrolase 1
	GART	2.64	Phosphoribosylglycinamide formyltransferase
	PAICS	1.79	Phosphoribosylaminoimidazole carboxylase
Unclassified	BANF1	2.77	Barrier to autointegration factor 1
	BAT1	1.95	HLA-B associated transcript 1///HLA-B associated transcript 1
	C1orf16	2.37	Chromosome 1 open reading frame 16
	CALU	2.40	Calumenin
	DAZAP2	2.57	DAZ associated protein 2
	DDX18	2.34	DEAD (Asp-Glu-Ala-Asp) box polypeptide 18
	DHX9	9.37	DEAH (Asp-Glu-Ala-His) box polypeptide 9
	EXOSC2	3.03	Exosome component 2
	FLJ10534	2.07	Hypothetical protein FLJ10534
	FLJ10719	2.42	Hypothetical protein FLJ10719
	FLJ12973	2.76	Hypothetical protein FLJ12973
	GANAB	2.07	Glucosidase, alpha; neutral AB
	HEM1	2.37	Hematopoietic protein 1
	IGHM	2.76	Anti-HIV-1 gp120 V3 loop antibody DO142-10 light chain variable region
	IGKC	3.15	Anti-rabies virus immunoglobulin rearranged kappa chain V-region
	LIN7C	3.51	lin-7 homolog C (*C. elegans*)
	LOC54499	2.31	Putative membrane protein
	M6PR	3.59	Mannose-6-phosphate receptor
	MGC8902	2.27	Hypothetical protein MGC8902/
	MOBK1B	2.67	MOB1, Mps one binder kinase activator-like 1B (yeast)
	NS	2.15	Nucleostemin
	NUSAP1	3.25	Nucleolar and spindle associated protein 1
	OK/SW-cl.56	1.85	Beta 5-tubulin
	OPRS1	2.76	Opioid receptor, sigma 1
	PEG 10	2.50	Paternally expressed 10
	PEX19	2.34	Peroxisomal biogenesis factor 19
	PGK1	2.11	Phosphoglycerate kinase 1
	RPE	2.35	Ribulose-5-phosphate-3-epimerase
	SDBCAG84	3.16	Serologically defined breast cancer antigen 84
	SMU1	2.70	smu-1 suppressor of mec-8 and unc-52 homolog (*C. elegans*)
	TAGLN2	2.03	Transgelin 2
	UBC	2.65	Ubiquitin C
	XPNPEP1	2.84	X-prolyl aminopeptidase
	YWHAE	6.39	Tyrosine 3-monooxygenase/tryptophan 5-monooxygenase activation protein, epsilon polypeptide
	YWHAZ	2.50	Tyrosine 3-monooxygenase/tryptophan 5-monooxygenase activation protein, zeta polypeptide

of $KBrO_3$ predominantly causes gross structural changes rather than small genetic changes such as point mutations.

$KBrO_3$ generates high yields of 8OHdG DNA adducts, which is a marker of oxidative DNA damage widely used as a predictor of carcinogenesis [10]. 8OHdG has been reported to be highly mutagenic in some experiments. In cell-free system, 8OHdG induced mutation by misincorporating adenine instead of cytosine [12]. Artificially incorporated 8OHdG at specific codons in a shuttle vector system efficiently induced GC > TA transversions in mammalian cells and *E. coli* [8,32,33]. In mammalian gene mutation assays in vitro and in vivo, however, the relationship between the accumulation of 8OHdG and the induction of GC > TA transversion has not been clear. Takeuchi et al.

Table 3
Genes whose expression was down-regulated by $KBrO_3$ (2.5 mM, 4 h)

	Gene symbol	Ratio	Gene title
Cell cycle, cell growth	FH	0.51	Fumarate hydratase
	MYC	0.55	v-myc myelocytomatosis viral oncogene homolog
Signal transduction	DUSP2	0.37	Dual specificityphosphatase 2
	RRBP1	0.39	Ribosome binding protein 1 homolog 180 kDa
	TBL3	0 43	Transducin (beta)-like3
Transcription regulation	CITED2	0.45	Cbp/p300-interacting transactivator, with Glu/Asp-rich carboxy-terminal domain, 2
	KIAA1196	0.43	KIAA1196 protein
	TZFP	0 39	Testis zinc finger protein
Chromosome organization	H1FX	0.14	H1 histone family member X
Protein modification	CLTB	0.43	Clathrin, light polypeptide (Lcb)
Energy pathway	FDX1	0.45	Ferredoxin 1
	QPRT	0.41	Quinolinate phosphoribosyltransferase
	SLC39A4	0.43	Solute carrier family 39 (zinc transporter), member 4
Unclassified	BTBD2	0.35	BTB (POZ) domain containing 2
	LOC339229	0.44	Hypothetical protein LOC339229
	MGRN1	0.44	Mahogunin, ring finger 1
	MRP63	0.41	Mitochondrial ribosomal protein 63
	PHLDA1	0.43	Pleckstrin homology-like domain, family A, member 1
	PTPLA	0.37	Protein tyrosine phosphatase-like (proline instead of catalytic arginine), member a
	SPATA2	0.45	Spermatogenesis associated 2

examined the mutagenicity of a hydroxyl radical generator, *N,N′*-bis (2-hydroxyperoxy-2-methoxyethyl)-1,4,5,8-naphthalene-tetra-carboxylic diimide (NP-III). Although NP-III highly produced 8OHdG upon irradiation with UV in V79 cells, the frequency of *Hprt* gene mutation was not significantly induced [34]. Molecular analysis demonstrated the no association of induction of 8OHdG with GC > TA transversion in the *Hprt* mutants [35]. 8OHdG is mainly removed by Ogg1 protein in a manor of the base excision repair (BER) pathway. Arai et al. investigated the relationship between the accumulation of oxidative DNA damage and the induction of gene mutation using *Ogg*1 deficient transgenic mice [36]. Although the 8OHdG level in kidneys of the *Ogg*1 deficient mice increase 200 times of the control level after 4 weeks' $KBrO_3$ treatment, the mutation frequency in the transgenic *gpt* gene was induced by less than 10 times of the control level. The molecular analysis revealed that the fraction of GC > TA transversions did not specifically increased. These results suggest that 8OHdG-mediated base substitutions do not mainly contribute to the mutagenic process involved in $KBrO_3$-induced carcinogenesis. Other genotoxic events must be involved in the carcinogenic process.

Our present studies strongly support this hypothesis. We demonstrated that $KBrO_3$ treatment clearly induced DNA damage in both the alkaline and neutral COM assay (Fig. 1). The alkaline COM assay is capable of detecting any DNA damages including DSB, single strand breaks (SSB), alkali-labile sites, DNA–DNA/DNA–protein cross-linking, and SSB associated with incomplete excision repair sites, while the neutral COM assay allows the detection of DSB, considered to be "biologically relevant" lesion of radiation damage [24]. $KBrO_3$ may have radio-mimic genotoxicity that yields oxidative DNA damage as well as DSB. $KBrO_3$ also induced MN formation and *TK* gene mutation significantly in TK6 cells. In the *TK* gene mutation assay, $KBrO_3$ predominantly produced SG mutants, but not NG mutants (Fig. 1c), implying that gross structural changes such as deletion and recombination are associated with the mutations. Molecular analysis of the *TK* mutants confirmed the assumption. Most of *TK* mutants showed LOH mutations, not non-LOH mutations, which are mainly point mutations. Harrington-Brock et al. also demonstrated that bromate compounds significantly induced *Tk* mutations in mouse lymphoma L5178Y cells, and almost all were LOH mutations [5]. LOH can be caused by deletions,

mitotic recombination between homologous alleles, or whole chromosome loss [20]. Molecular analysis can distinguish between them and reveal the mechanism and the characteristics of the mutants. In this study, $KBrO_3$ predominantly induced large deletions that resulted in hemizygous LOH (Table 1). The large deletions were mainly terminal deletions in the proximal region of chromosome 17q, which were rarely observed in spontaneously arising *TK* mutants (Fig. 3). The mutational spectrum and LOH pattern induced by $KBrO_3$ were similar to those induced by X-irradiation (Figs. 2 and 3) [20,21]. DSBs induced X-rays cause large deletions [19,20]. When the DSBs are repaired by the non-homologous end-joining pathway, interstitial deletions result. The broken chromosome ends can be also stabilized by the addition of new telomere sequences. Because TK6 cells have high telomerase activity [20], the result is terminal deletions. Thus, the major genotoxicity of $KBrO_3$ may be due to DSBs, but not to 8OHdG converting GC > TA transversion.

Some 8OHdG lesions can convert DSBs through the BER pathway [37]. In the initial step of BER, Ogg1 removes 8OHdG by DNA glycosylase activity and nicks the DNA backbone because of its associated lyase activity. The resulting SSB is processed by an apurinic endonuclease, which generates a single nucleotide gap. The gap is filled in by a DNA polymerase and sealed by a DNA ligase [38]. Clustered 8OHdG lesions induced by $KBrO_3$ may not be appropriately repaired by BER and cause DSB, however, because it is possible that two closely opposed 8OHdGs convert two closely opposed SSBs by BER resulting DSB [39,40]. Yang et al. developed Ogg1 over-expressing TK6 cell (TK6-hOGG1) and examined cytotoxic and mutagenic responses to gamma-irradiation [41]. They demonstrated that TK6-hOGG1 cells are more sensitive than the parental TK6 cells to cytotoxicity and mutagenicity by gamma-irradiation, and most of the induced *TK* mutants in TK6-OGG1 exhibited SG phenotype, which were probably large deletion mutants resulted by DSBs. This result clearly indicates that BER pathway contributes to convert oxidative damages to DSBs. Some clustered 8OHdG induced by $KBrO_3$ may covert to DSBs in TK6 cells, because TK6 is Ogg1 proficient cells [37].

To clarify the genotoxic characteristics of $KBrO_3$, we investigated the gene expression profile using Affymetrix GeneChip® Expression analysis. Many genes were up- or down-regulated by exposure to 2.5 mM $KBrO_3$ (Tables 2 and 3). Akerman et al. investigated the alterations of gene expression profiles in ionizing radiation-exposed TK6 cells [42]. They reported a >50% increase in expression of ATF-3 (stress response), Cyclin G (cell cycle), FAS antigen (apoptosis), GADD45 (repair and apoptosis), PCNA (repair), Rad51 (repair), and p21 (cell cycle) and a 40% decrease in expression of c-Myc (transcription factor), interferon stimulatory gene factor-3 (cell signaling), and p55CDC (cell cycle). We also observed up-regulation of p21 and down-regulation of c-Myc. Up-regulation of p21, however, is observed in TK6 cells exposed to any DNA-damaging chemical [43]. Islaih et al. also demonstrated the relationship between the gene expression profiles and the DNA damaging agents using TK6 cells [43]. They examined six chemicals including H_2O_2 and bleomycin which induce oxidative DNA damage. Although 10 genes were commonly up-regulated between H_2O_2 and bleomycin treatments, these genes except for p21 were not observed in our experiment. Thus, we could not find the similarity of gene expression profile by the treatment with $KBrO_3$ to by the treatment with ionizing radiation as well as oxidative damage inducers. Comparing gene expression profiles across platforms, laboratories, and experiments must be difficult [44]. Although it is difficult to judge from the expression analysis of the single chemical, information on genes which altered their expression gives a clue to understand the mechanism of action. Firstly, predominance of DNA repair and cell cycle related genes in up-regulated genes supports the genotoxic action of $KBrO_3$. Up-regulation of stress genes and apoptosis related genes suggests an involvement of oxidative stress. Up-regulation of catalase may be responsible for the oxidative damage by $KBrO_3$ (Table 2). Unclassified genes for alteration may have a functional relationship with genotoxic mechanism.

In conclusion, $KBrO_3$ predominantly induced large deletions at chromosomal level in human TK6 cells. The major genotoxicity leading to carcinogenesis of $KBrO_3$ may be due to DSBs rather than to 8OHdG adducts that lead to GC > TA transversions, as is commonly believed.

Acknowledgments

The TK6 cell line used in this study was a kind gift of Dr. John B. Little of the Harvard School of Public Health, Boston, MA. This study was supported by Health, Welfare, and Labor Science Research Grants (H15-chem-002, H15-food-004) in Japan.

References

[1] Y. Kurokawa, A. Maekawa, M. Takahashi, Y. Hayashi, Toxicity and carcinogenicity of potassium bromate—a new renal carcinogen, Environ. Health Perspect. 87 (1990) 309–335.

[2] Y. Kurokawa, S. Aoki, Y. Matsushima, N. Takamura, T. Imazawa, Y. Hayashi, Dose–response studies on the carcinogenicity of potassium bromate in F344 rats after long-term oral administration, J. Natl. Cancer Inst. 77 (1986) 977–982.
[3] A.B. DeAngelo, M.H. George, S.R. Kilburn, T.M. Moore, D.C. Wolf, Carcinogenicity of potassium bromate administered in the drinking water to male B6C3F1 mice and F344/N rats, Toxicol. Pathol. 26 (1998) 587–594.
[4] M. Ishidate Jr., K. Yoshikawa, Chromosome aberration tests with Chinese hamster cells in vitro with and without metabolic activation—a comparative study on mutagens and carcinogens, Arch. Toxicol. Suppl. 4 (1980) 41–44.
[5] K. Harrington-Brock, D.D. Collard, T. Chen, Bromate induces loss of heterozygosity in the thymidine kinase gene of L5178Y/Tk(±)-3.7.2C mouse lymphoma cells, Mutat. Res. 537 (2003) 21–28.
[6] M. Hayashi, T. Sofuni, M. Ishidate Jr., High-sensitivity in micronucleus induction of a mouse strain (MS), Mutat. Res. 105 (1982) 253–256.
[7] M. Hayashi, M. Kishi, T. Sofuni, M. Ishidate Jr., Micronucleus tests in mice on 39 food additives and eight miscellaneous chemicals, Food Chem. Toxicol. 26 (1988) 487–500.
[8] H. Kamiya, K. Miura, H. Ishikawa, H. Inoue, S. Nishimura, E. Ohtsuka, c-Ha-ras containing 8-hydroxyguanine at codon 12 induces point mutations at the modified and adjacent positions, Cancer Res. 52 (1992) 3483–3485.
[9] A.G. Knudson, Antioncogenes and human cancer, Proc. Natl. Acad. Sci. U.S.A. 90 (1993) 10914–10921.
[10] H. Kasai, S. Nishimura, Y. Kurokawa, Y. Hayashi, Oral administration of the renal carcinogen, potassium bromate, specifically produces 8-hydroxydeoxyguanosine in rat target organ DNA, Carcinogenesis 8 (1987) 1959–1961.
[11] K.C. Cheng, D.S. Cahill, H. Kasai, S. Nishimura, L.A. Loeb, 8-Hydroxyguanine, an abundant form of oxidative DNA damage, causes G–T and A–C substitutions, J. Biol. Chem. 267 (1992) 166–172.
[12] S. Shibutani, M. Takeshita, A.P. Grollman, Insertion of specific bases during DNA synthesis past the oxidation-damaged base 8-oxodG, Nature 349 (1991) 431–434.
[13] K. Sai, C.A. Tyson, D.W. Thomas, J.E. Dabbs, R. Hasegawa, Y. Kurokawa, Oxidative DNA damage induced by potassium bromate in isolated rat renal proximal tubules and renal nuclei, Cancer Lett. 87 (1994) 1–7.
[14] G. Speit, S. Haupter, P. Schutz, P. Kreis, Comparative evaluation of the genotoxic properties of potassium bromate and potassium superoxide in V79 Chinese hamster cells, Mutat. Res. 439 (1999) 213–221.
[15] T. Umemura, K. Sai, A. Takagi, R. Hasegawa, Y. Kurokawa, A possible role for oxidative stress in potassium bromate (KBrO3) carcinogenesis, Carcinogenesis 16 (1995) 593–597.
[16] K. Fujie, H. Shimazu, M. Matsuda, T. Sugiyama, Acute cytogenetic effects of potassium bromate on rat bone marrow cells in vivo, Mutat. Res. 206 (1988) 455–458.
[17] M. Ishidate Jr., T. Sofuni, K. Yoshikawa, M. Hayashi, T. Nohmi, M. Sawada, A. Matsuoka, Primary mutagenicity screening of food additives currently used in Japan, Food Chem. Toxicol. 22 (1984) 623–636.
[18] H.L. Liber, W.G. Thilly, Mutation assay at the thymidine kinase locus in diploid human lymphoblasts, Mutat. Res. 94 (1982) 467–485.
[19] H.L. Liber, D.W. Yandell, J.B. Little, A comparison of mutation induction at the tk and hprt loci in human lymphoblastoid cells; quantitative differences are due to an additional class of mutations at the autosomal tk locus, Mutat. Res. 216 (1989) 9–17.
[20] M. Honma, Generation of loss of heterozygosity and its dependency on p53 status in human lymphoblastoid cells, Environ. Mol. Mutagen. 45 (2005) 162–176.
[21] M. Honma, M. Hayashi, T. Sofuni, Cytotoxic and mutagenic responses to X-rays and chemical mutagens in normal and p53-mutated human lymphoblastoid cells, Mutat. Res. 374 (1997) 89–98.
[22] L. Zhan, H. Sakamoto, M. Sakuraba, D.S. Wu, L.S. Zhang, T. Suzuki, M. Hayashi, M. Honma, Genotoxicity of microcystin-LR in human lymphoblastoid TK6 cells, Mutat. Res. 557 (2004) 1–6.
[23] N. Koyama, H. Sakamoto, M. Sakuraba, T. Koizumi, Y. Takashima, M. Hayashi, H. Matsufuji, K. Yamagata, S. Masuda, N. Kinae, M. Honma, Genotoxicity of acrylamide and glycidamide in human lymphoblastoid TK6 cells, Mutat. Res. 603 (2006) 151–158.
[24] S. Wada, H. Kurahayashi, Y. Kobayashi, T. Funayama, K. Yamamoto, M. Natsuhori, N. Ito, The relationship between cellular radiosensitivity and radiation-induced DNA damage measured by the comet assay, J. Vet. Med. Sci. 65 (2003) 471–477.
[25] M. Watanabe-Akanuma, T. Ohta, Y.F. Sasaki, A novel aspect of thiabendasole as a photomutagen in bacteria and cultured human cells, Mutat. Res. 158 (2005) 213–219.
[26] T. Matsushima, M. Hayashi, A. Matsuoka, M. Ishidate Jr., K.F. Miura, H. Shimizu, Y. Suzuki, K. Morimoto, H. Ogura, K. Mure, K. Koshi, T. Sofuni, Validation study of the in vitro micronuclei test in a Chinese hamster lung cell line (CHL/IU), Mutagenesis 14 (1999) 569–580.
[27] T. Omori, M. Honma, M. Hayashi, Y. Honda, I. Yoshimura, A new statistical method for evaluating of L5178Ytk± mammalian cell data using microwell method 517 (2002) 199–208.
[28] M. Honma, M. Momose, H. Tanabe, H. Sakamoto, Y. Yu, J.B. Little, T. Sofuni, M. Hayashi, Requirement of wild-type p53 protein for maintenance of chromosomal integrity, Mol. Carcinog. 28 (2000) 203–214.
[29] P.L. Olive, DNA damage and repair in individual cells: applications of the comet assay in radiobiology, Int. J. Radiat. Biol. 75 (1999) 395–405.
[30] D.E. Levin, M. Hollstein, M.F. Christman, E.A. Schwiers, B.N. Ames, A new Salmonella tester strain (TA102) with A X T base pairs at the site of mutation detects oxidative mutagens, Proc. Natl. Acad. Sci. U.S.A. 79 (1982) 7445–7449.
[31] T. Arai, V.P. Kelly, O. Minowa, T. Noda, S. Nishimura, High accumulation of oxidative DNA damage, 8-hydroxyguanine, in Mmh/Ogg1 deficient mice by chronic oxidative stress, Carcinogenesis 23 (2002) 2005–2010.
[32] F. Le Page, A. Margot, A.P. Grollman, A. Sarasin, A. Gentil, Mutagenicity of a unique 8-oxoguanine in a human Ha-ras sequence in mammalian cells, Carcinogenesis 16 (1995) 2779–2784.
[33] M.L. Wood, M. Dizdaroglu, E. Gajewski, J.M. Essigmann, Mechanistic studies of ionizing radiation and oxidative mutagenesis: genetic effects of a single 8-hydroxyguanine (7-hydro-8-oxoguanine) residue inserted at a unique site in a viral genome, Biochemistry 29 (1990) 7024–7032.
[34] T. Takeuchi, S. Matsugo, K. Morimoto, Mutagenicity of oxidative DNA damage in Chinese hamster V79 cells, Carcinogenesis 18 (1997) 2051–2055.
[35] M. Nakajima, T. Takeuchi, K. Ogino, K. Morimoto, Lack of direct involvement of 8-hydroxy-2′-deoxyguanosine in

hypoxanthine-guanine phosphoribosyltransferase mutagenesis in V79 cells treated with *N,N'*-bis(2-hydroxyperoxy-2-methoxy-ethyl)-1,4,5,8-naphthalenetetracarboxyli c-diimide (NP-III) or riboflavin, Jpn. J. Cancer Res. 93 (2002) 247–252.

[36] T. Arai, V.P. Kelly, K. Komoro, O. Minowa, T. Noda, S. Nishimura, Cell proliferation in liver of Mmh/Ogg1-deficient mice enhances mutation frequency because of the presence of 8-hydroxyguanine in DNA, Cancer Res. 63 (2003) 4287–4292.

[37] N. Yang, M.A. Chaudhry, S.S. Wallace, Base excision repair by hNTH1 and hOGG1: a two edged sword in the processing of DNA damage in gamma-irradiated human cells, DNA Repair (Amst.) 5 (2006) 43–51.

[38] G. Slupphaug, B. Kavli, H.E. Krokan, The interacting pathways for prevention and repair of oxidative DNA damage, Mutat. Res. 531 (2003) 231–251.

[39] K. Tian, M. McTigue, S.C. de los, Sorting the consequences of ionizing radiation: processing of 8-oxoguanine/abasic site lesions, DNA Repair (Amst.) 1 (2002) 1039–1049.

[40] M.E. Lomax, S. Cunniffe, P. O'Neill, Efficiency of repair of an abasic site within DNA clustered damage sites by mammalian cell nuclear extracts, Biochemistry 43 (2004) 11017–11026.

[41] N. Yang, H. Galick, S.S. Wallace, Attempted base excision repair of ionizing radiation damage in human lymphoblastoid cells produces lethal and mutagenic double strand breaks, DNA Repair (Amst.) 3 (2004) 1323–1334.

[42] G.S. Akerman, B.A. Rosenzweig, O.E. Domon, C.A. Tsai, M.E. Bishop, L.J. McGarrity, J.T. Macgregor, F.D. Sistare, J.J. Chen, S.M. Morris, Alterations in gene expression profiles and the DNA-damage response in ionizing radiation-exposed TK6 cells, Environ. Mol. Mutagen. 45 (2005) 188–205.

[43] M. Islaih, B.W. Halstead, I.A. Kadura, B. Li, J.L. Reid-Hubbard, L. Flick, J.L. Altizer, D.J. Thom, D.K. Monteith, R.K. Newton, D.E. Watson, Relationships between genomic, cell cycle, and mutagenic responses of TK6 cells exposed to DNA damaging chemicals, Mutat. Res. 578 (2005) 100–116.

[44] C.L. Yauk, M.L. Berndt, A. Williams, G.R. Douglas, Comprehensive comparison of six microarray technologies, Nucleic Acids Res. 32 (2004) e124.

SETAC PRESS

Environmental Toxicology and Chemistry, Vol. 26, No. 7, pp. 1370–1379, 2007

Printed in the USA
0730-7268/07 $12.00 + .00

ARYL HYDROCARBON RECEPTOR LIGAND ACTIVITY OF POLYCYCLIC AROMATIC KETONES AND POLYCYCLIC AROMATIC QUINONES

KENTARO MISAKI,†‡ HIROFUMI KAWAMI,§ TOTA TANAKA,§ YOJI HANDA,‖ MASAFUMI NAKAMURA,‖ SABURO MATSUI,‡ and TOMONARI MATSUDA*‡

†Department of Environmental Engineering, Kyoto University, Yoshidahonmachi, Kyoto, Japan
‡Graduate School of Global Environmental Studies, Kyoto University, Yoshidahonmachi, Kyoto, Japan
§Research Center for Environmental Quality Control, Kyoto University, Yumihama 1-3, Otsu, Japan
‖Hiyoshi Corporation, Kitanosho-cho 908, Omihachiman, Shiga, Japan

(*Received* 8 *September* 2006; *Accepted* 26 *January* 2007)

Abstract—Polycyclic aromatic ketones (PAKs) and polycyclic aromatic quinones (PAQs) are oxygenated polycyclic aromatic hydrocarbons (PAHs), and reports about the aryl hydrocarbon receptor (AhR) ligand activities of these compounds are few. In this study, activation of AhR by 41 polycyclic aromatic compounds (PACs), focusing especially on PAKs and PAQs, was determined by measuring β-galactosidase activity from a reporter plasmid in yeast engineered to express human AhR and the AhR nuclear translocator proteins and by measuring luciferase activity from mouse hepatoma (H1L1) cells (chemical-activated luciferase expression [CALUX] assay). The PACs used in these experiments included 11 PAKs, seven PAQs, and 21 PAHs. In this study, the PAKs 11*H*-benzo[*a*]fluoren-11-one (B[*a*]FO), 11*H*-benzo[*b*]fluoren-11-one (B[*b*]FO) and 7*H*-benzo[*c*]fluoren-7-one and the PAQs 5,12-naphthacenequinone, 1,4-chrysenequinone, and 7,12-benz[*a*]anthracenequinone showed high AhR activities in H1L1 cells, although these values were not as high as that for benzo[*a*]pyrene (B[*a*]P). These PAKs and PAQs showed significantly stronger activities in yeast cells relative to B[*a*]P. It was predicted that PAKs such as B[*a*]FO and B[*b*]FO occupied 0.06% to 1.3% of the total induction equivalents, and each contribution matched the contribution of PAHs such as B[*a*]P, chrysene, and benz[*a*]anthracene in gasoline exhaust particulates and airborne particulates using data of CALUX assay.

Keywords—Polycyclic aromatic ketone Polycyclic aromatic quinone Aryl hydrocarbon receptor activity Reporter gene assay

INTRODUCTION

In the atmospheric and aquatic environments, various polycyclic aromatic hydrocarbons (PAHs) originally derived from oil fuel and its combustion are detected at high levels [1–4], and some wildlife and humans are at risk of exposure to them. High-molecular-weight polycyclic aromatic hydrocarbons (PAHs) easily accumulate, mainly in fatty tissues, through biological concentration in ecological systems, which is likely to cause ill effects on the health and life span of exposed animals [5].

Many studies have been made of PAH mutagenicity and carcinogenicity. The aryl hydrocarbon receptor (AhR) recognizes PAHs as exogenous ligands, and that induces enzymes, such as cytochrome P450s (CYPs). This leads to the metabolism of PAHs and the formation of DNA adducts with PAHs [6]. Many potent AhR-active PAHs also are potent inducers of DNA damage, although mutagenic potency is not necessarily proportional to the AhR-inducing potency [6].

Since the 1990s, some studies regarding endocrine-disrupting activity in the atmospheric environment have been performed. Endocrine-disrupting phenomena by diesel exhaust often have been reported for male mice and rats [7,8]. Male ICR mice (age, 6 weeks) exposed to diesel exhaust showed ultrastructural changes in Leydig cells, increases in the density of Leydig cells in the testes, decreases in the ability of sperm movement, and reduction in sperm production [7]. Inhalation of diesel exhaust reduced sperm production and decreased numbers of spermatids in tubules of growing male F344 rats [8]. Diesel exhaust may be related mainly to antiandrogenic and estrogenic activity [9–12]. It also was indicated that the mass of storage tissue and production of gametes decreased significantly and in a concentration-dependent manner in marine mollusks exposed to diesel oil [5]. These endocrine disruption activities of diesel exhaust and oil likely are caused by PAHs such as benzo[*a*]pyrene (B[*a*]P); however, it has not yet been elucidated what compounds contribute most to this activity [9–12]. It was shown that exposure to some PAHs and hydroxylated PAHs resulted in estrogenic activity for culture cells via direct binding to estrogen receptor [12,13]. To the contrary, it also is thought that PAHs cause endocrine disruption via AhR and that the induction of enzymes, such as CYP1A1, mediated by AhR likely is one of the biomarkers related to endocrine disruption [9–12]. Several possible mechanisms of AhR-mediated antiandrogenic activity have been proposed [9,10]. Okamura et al. [9] have reported that in reporter gene assays using prostate cancer cells, significant correlations between antiandrogenic and AhR agonistic activities were demonstrated with 100 nM of several PAHs, and Kizu et al. [10] have suggested that the ligand-binding AhR contributed to the inhibition of gene transcription by androgen receptor in prostate cancer cells. In addition, it has been predicted that endocrine-disrupting activity in male reproductive organs, as mediated by estrogen receptor–AhR binding interaction with PAH exposure, may occur [11].

The AhR is present in cytoplasm as a complex with dimeric heat shock protein 90 before ligand interaction. A ligand activates AhR, and AhR transfers into the nucleus and interacts

* To whom correspondence may be addressed (matsuda@eden.env.kyoto-u.ac.jp).

with the AhR nuclear translocator to form a heterodimeric transcription factor called the AhR complex. The AhR complex binds xenobiotic response elements (XREs) and mediates the regulation of gene expression. The AhR complex enhances transcription of many genes, including specific CYPs, glutathione-*S*-transferases, NAD(P)H-dependent quinone oxidoreductase 1, growth factors, and cytokines [14]. Many environmental pollutants or natural substances (e.g., dioxins, PAHs, and tryptophan derivatives) bind and activate AhR as exogenous or endogenous ligands [6,9,12,14–22].

In the atmospheric environment, diesel exhaust, airborne particles, and oxygenated PAHs, such as polycyclic aromatic ketones (PAKs) and polycyclic aromatic quinones (PAQs), also are included as abundant as PAHs [1–3]; however, the toxicological significance of these compounds is not well elucidated [6,23,24]. The AhR ligand activities of PAHs using various kinds of species (e.g., yeast, mouse, rat, human, and fish) and cells with various detection methods (AhR ligand-binding assay, reporter gene assay, CYP1A mRNA and protein quantification, and CYP1A activity detection [e.g., AHH activity and EROD activity]) have been measured [6,9,12,14–22], whereas the reports about AhR activation of PAKs and PAQs are few [12]. Machala et al. [12] showed that the value of AhR ligand activity for one PAQ, 7,12-benz[*a*]anthracenequinone (BAQ), was two orders of magnitude lower than that for B[*a*]P. In our previous study, the mRNA induction of AhR-regulated metabolic enzymes (e.g., CYP1A1) by PAQs and PAKs in HepG2 cells was reported, and it was first found that 5,12-naphthacenequinone (NCQ) and 11*H*-benzo[*b*]fluoren-11-one (B[*b*]FO) showed CYP1A1 mRNA induction [25].

In the present study, activation of AhR by polycyclic aromatic compounds (PACs), which include PAKs, PAQs, and PAHs (as shown in Fig. 1), was determined by β-galactosidase activity from a reporter plasmid in yeast developed by Miller [14] that was engineered to express human AhR and AhR nuclear translocator proteins and by luciferase activity in mouse hepatoma (H1L1) cells (the chemical activated luciferase gene expression [CALUX] assay) developed by Denison et al. [19]. Then, the AhR activity by these two methods and previous data about CYP1A1 mRNA induction in HepG2 cells were compared for each chemical [25]. Considering metabolism, liver cells are appropriate for examining AhR activity of PACs, although it is important to examine the AhR activity of PACs by using target organ cells in each toxicity [6,9,12,14–22]. Additionally, the contribution of each PAC to the AhR activity of atmospheric environmental pollutants was evaluated using data about AhR activity of PACs in CALUX assay [1,3]. The chemicals used in the present experiments were 41 PACs, including 11 PAKs, seven PAQs, and 21 PAHs.

MATERIALS AND METHODS

Chemicals

2,3,7,8-Tetrachlorodibenzo-*p*-dioxin (TCDD) was supplied by Cambridge Isotope Laboratories (Andover, MA, USA). Most PACs were supplied by Sigma-Aldrich (St. Louis, MO, USA). The other PACs were supplied by Nacalaitesque (Tokyo, Japan), Wako Chemical (Osaka, Japan), Tokyo Kasei (Tokyo, Japan), and Promochem (Wesel, Germany). The purity of many PACs was 99 to 100%. The purities of benzo[*b*]fluoranthene (B[*b*]FA), benzo[*k*]fluoranthene (B[*k*]FA), 3-methylcholanthrene (3-MC), benzo[*ghi*]perylene (B[*ghi*]Pe), naphtho[2,3-*a*]pyrene (N[*a*]P), anthraquinone, BAQ, and β-naphthoflavone (β-NF) were 98%. The purities of triphenylene, dibenz[*a,h*]anthracene (DB[*a,h*]A), dibenz[*a,c*]anthracene, phenalenone (PhO), xanthone, thioxanthone, NCQ, and alizarine (Alz) were 97%. The purity of benzo[*b*]fluorene (B[*b*]F) was 95%. Phenol, toluene, and bromobenzene were supplied by Wako Chemical.

11*H*-Benzo[*a*]fluoren-11-one (B[*a*]FO), B[*b*]FO, 7*H*-benzo[*c*]fluoren-7-one (B[*c*]FO), cyclopenta[*cd*]pyren-3(4*H*)-one (CPPO), and 6*H*-benzo[*cd*]pyren-6-one (BPO) were synthesized as described previously [26–29]. These compounds were purified by column chromatography and recrystallization. Only the purity of B[*c*]FO was 98%; the purities of the other four synthesized compounds were greater than 99% as judged by high-performance liquid chromatography (HPLC).

Yeast assay

Saccharomyces cerevisiae strain YCM3 was grown in synthetic glucose medium at 30°C overnight in a shaking incubator [14]. The next day, 10 μl from the saturated culture were inoculated into glass tubes containing 400 μl of a synthetic, 2% galactose medium. Test compounds dissolved in 2 μl of dimethyl sulfoxide were added to the medium to achieve a final solvent concentration of 0.5%, followed by an 18-h incubation at 30°C. The cell densities were determined by reading the absorbance at 595 nm, and 10 μl of the cell suspension were added to 140 μl of Z-buffer (60 mM Na_2HPO_4, 40 mM NaH_2PO_4, 1 mM $MgCl_2$, 10 mM KCl, 2 mM dithiothreitol, and 0.2% sarkosyl). The reaction was started by adding 50 μl of *o*-nitrophenyl-β-D-galactopyranoside (4 mg/ml solution in Z-buffer). The samples were incubated at 37°C for 60 min. Absorbances of the reaction mixture were read in a spectrophotometer at 405 nm. The activity of β-galactosidase (referred to as lacZ units) was calculated by the following formula: $412 \cdot A_{405nm}/(400 \cdot A_{595nm} \cdot$milliliters of cell suspension added·minutes of reaction time). The concentrations producing galactosidase activity equal to 25% of the maximal response to TCDD (EC_{TCDD25}) were calculated. The ratios of the EC_{TCDD25} of B[*a*]P to the EC_{TCDD25} of each of the compounds were calculated and referred to as induction equivalency factors (IEFs). For expression of AhR activity, the median effect concentration (EC50) of each chemical generally is used. The EC50, however, is dependent on the maximal response. In addition, this maximal value changes corresponding to each compound, because many ligands show cytotoxicity or cannot be dissolved in medium at high concentration and the factual maximal activity value cannot be detected. In the contrary, activity values at each EC_{TCDD25} concentration are constant, so in the present research, the EC_{TCDD25} was used for determination of the strength of AhR activity [16,17,22].

CALUX assay

Mouse hepatoma (H1L1.1c2) cells (~1.5×10^5 cells/well) were cultured in 96-well culture plates, and samples dissolved in dimethyl sulfoxide were added to the medium to achieve a final solvent concentration of 1% [16,22]. After the plates were incubated at 37°C in 5% CO_2 for 24 h, the cell viability was confirmed under a microscope. Subsequently, the medium was removed, and the cells were lysed. Adding luciferin as the substrate, the luciferase activity was determined under a luminometer and reported as relative light units. The concentrations producing luciferase activity equal to 25% of the maximal response to TCDD were calculated and also referred to as the EC_{TCDD25}. The ratios of the EC_{TCDD25} of B[*a*]P to the

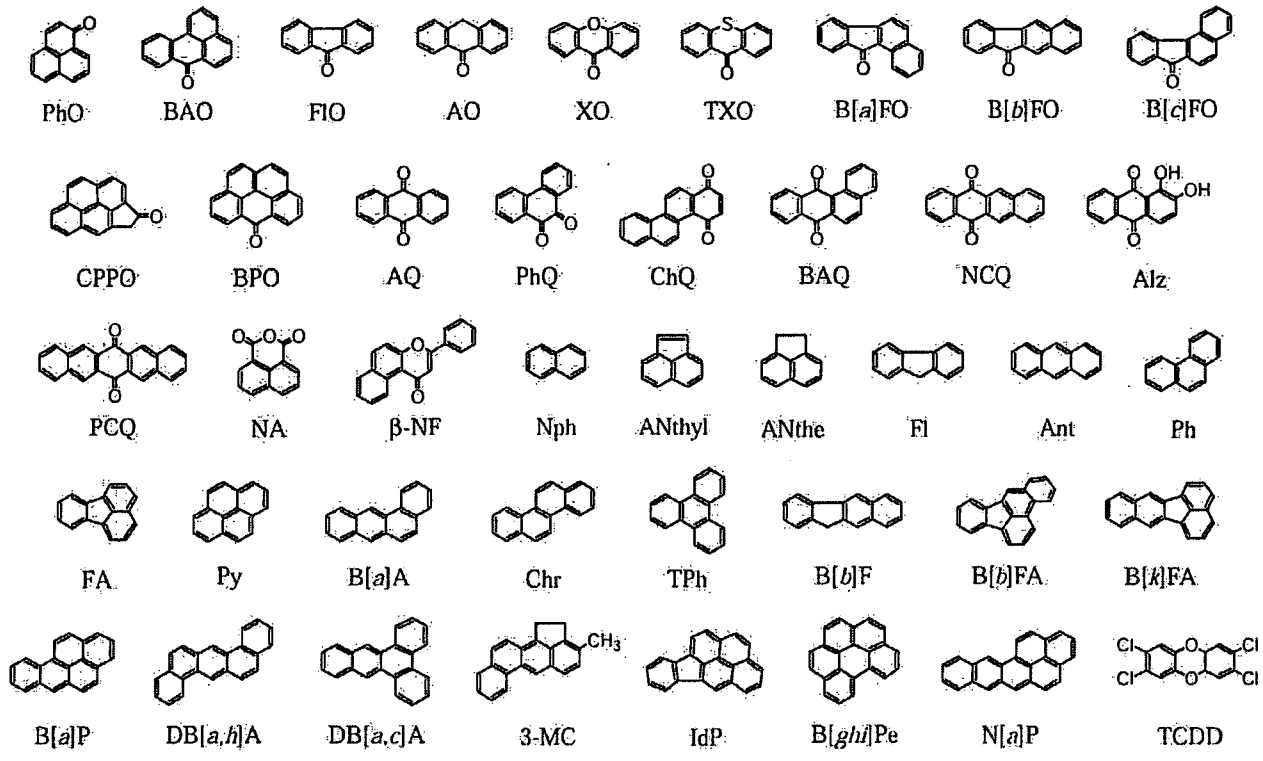

Fig. 1. Chemical structures of polycyclic aromatic compounds (PACs) under study and 2,3,7,8-tetrachlorodibenzo-*p*-dioxin (TCDD). PhO = phenalenone; BAO = 7*H*-benz[*de*]anthracen-7-one; FlO = fluorenone; AO = anthrone; XO = xanthone; TXO = thioxanthone; B[*a*]FO = 11*H*-benzo[*a*]fluoren-11-one; B[*b*]FO = 11*H*-benzo[*b*]fluoren-11-one; B[*c*]FO = 7*H*-benzo[*c*]fluoren-7-one; CPPO = cyclopenta[*cd*]pyren-3[4*H*]-one; BPO = 6*H*-benzo[*de*]pyren-6-one; AQ = anthraquinone; PhQ = phenanthrenequinone; ChQ = 1,4-chrysenequinone; BAQ = 7,12-benz[*a*]anthracenequinone; NCQ = 5,12-naphthacenequinone; Alz = alizarin; PCQ = pentacenequinone; NA = 1,8-naphthalic anhydride; β-NF = β-naphthoflavone; Nph = naphthalene; ANthyl = acenaphthylene; ANthe = acenaphthene; Fl = fluorene; Ant = anthracene; Ph = phenanthrene; FA = fluoranthene; = pyrene; B[*a*]A = benz[*a*]anthracene; Chr = chrysene; TPh = triphenylene; B[*b*]F = benzo[*b*]fluorene; B[*b*]FA = benzo[*b*]fluoranthene; B[*k*]FA = benzo[*k*]fluoranthene; B[*a*]P = benzo[*a*]pyrene; DB[*a,h*]A = dibenz[*a,h*]anthracene; DB[*a,c*]A = dibenz[*a,c*]anthracene; 3-MC = 3-methylcholanthrene; IdP = indeno[1,2,3-*cd*]pyrene; B[*ghi*]Pe = benzo[*ghi*]perylene; N[*a*]P = naphtho[2,3-*a*]pyrene.

EC_{TCDD25} of each of the compounds were calculated and referred to as IEFs.

Hydrophobicity

The value of log K_{OW} for oxygenated PAHs and several PAHs was calculated from the standard line, which is drawn using log K_{OW} and the retention times in reversed-phase HPLC for standard compounds according to the method of Sarna et al. [30]. The HPLC system constituted Shimpack FC-ODS column (ø4.6 × 150 mm; Shimadzu, Kyoto, Japan), LC-10ATvp pump, SIL-10ADvp autoinjector, SPD-M10Avp UV-VIS detector at 254 nm, and SCL-10Avp system controller (all appliances were from Shimadzu). The mobile phase used was methanol–water (90:10) at a flow rate of 1.0 ml/min. The data of K_{OW} for phenol, toluene, bromobenzene, and several PAHs were used for constructing the standard line [31,32].

RESULTS

Yeast assay

The AhR ligand activity was examined with a yeast reporter gene assay using the YCM3, in which the human AhR and AhR nuclear translocator were recombined [14]. This yeast was exposed to chemicals, after which heterodimer AhR complex was formed and transactivation by AhR complex was assessed by β-galactosidase activity using pTXRE5-Z [14]. In the present research, glass tubes were used for the culture of yeast, because TCDD and PAHs preferentially adhered to plastic surfaces. The AhR activity of such compounds for yeast cultured in a plastic tube decreased by approximately one order of magnitude lower than for yeast cultured in a glass tube. The solubility of TCDD may be the factor that limits the magnitude of the response [14]. The value of the 25% effect concentration (EC25) for TCDD (1.3 nM) was slightly lower than that for B[*a*]P (EC_{TCDD25} = 4.5 nM) (Fig. 2 and Table 1).

The AhR ligand activity of oxygenated PAHs, such as PAKs and PAQs, is shown in Figure 2A–C and Table 1. The AhR ligand activities of four-ring NCQ (EC_{TCDD25} = 88 pM), BAQ (EC_{TCDD25} = 280 pM), B[*b*]FO (EC_{TCDD25} = 350 pM), and B[*a*]FO (EC_{TCDD25} = 720 pM) were stronger than that of B[*a*]P (Fig. 2B and C). The AhR ligand activities of four-ring B[*c*]FO (EC_{TCDD25} = 17 nM) and 7*H*-benz[*de*]anthracen-7-one (BAO; EC_{TCDD25} = 20 nM), and 5-ring CPPO (EC_{TCDD25} = 24 nM) were potencies one order of magnitude lower than that of B[*a*]P (Fig. 2A and B). Two- and three-ring PAKs and PAQs showed potencies two or three orders of magnitude lower than that of B[*a*]P (Fig. 2A and C). Five-ring BPO showed a potency two orders of magnitude lower than that of B[*a*]P (EC_{TCDD25} = 320 nM) (Fig. 2B), and five-ring pentacenequinone (PCQ) did not induce AhR ligand activity (Fig. 2C). One of the dyes and one of the photomodified PAHs, Alz [33], showed a potency two orders of magnitude lower than that of B[*a*]P (EC_{TCDD25} = 150 nM) (Fig. 2C) [22]. Representative AhR ligand β-NF, which

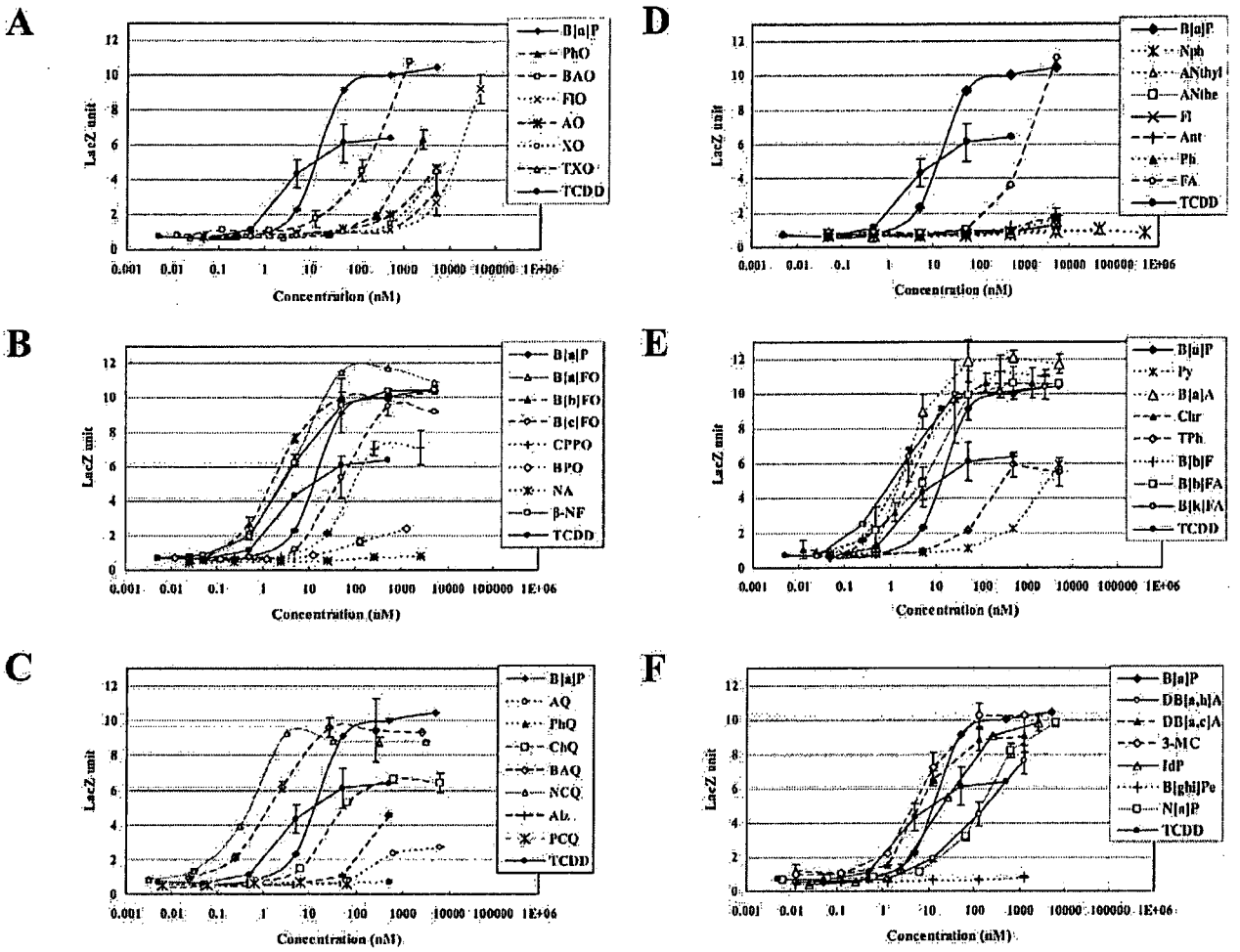

Fig. 2. β-Galactosidase activity in the yeast system. Yeast was treated for 18 h with polycyclic aromatic compounds (PACs) and 2,3,7,8-tetrachloride-*p*-dioxin (TCDD). See Figure 1 for acronyms of test compounds.

was used for comparison (β-NF is not an atmospheric pollutant), showed a higher potency (EC_{TCDD25} = 550 pM) than that of B[*a*]P (Fig. 2B)

The AhR ligand activity of PAHs also is shown in Figure 2D–F and in Table 1. Five-ring B[*k*]FA (EC_{TCDD25} = 200 pM) and B[*b*]FA (EC_{TCDD25} = 1.5 nM) and four-ring chrysene (Chr; EC_{TCDD25} = 680 pM), benz[*a*]anthracene (B[*a*]A; EC_{TCDD25} = 1.1 nM) and B[*b*]F (EC_{TCDD25} = 330 pM) also were more potent AhR agonists than B[*a*]P (Fig. 2E). High-ring-number PAHs, such as DB[*a,h*]A (EC_{TCDD25} = 15 nM), indeno[1,2,3-*cd*]pyrene (IdP; EC_{TCDD25} = 4.8 nM) and N[*a*]P (EC_{TCDD25} = 30 nM) were less potent than B[*a*]P (Fig. 2F). Two- and three-ring PAHs either did not show AhR activity or showed only low activities (<25% of maximal activity of TCDD) (Fig. 2D). Four-ring fluoranthene (FA; EC_{TCDD25} = 240 nM), pyrene (EC_{TCDD25} = 400 nM), and (EC_{TCDD25} = 49 nM) showed potencies two orders of magnitude lower than B[*a*]P (Fig. 2D and E). Six-ring B[*ghi*]Pe did not induce AhR activity (Fig. 2F).

Significant inhibition of yeast cell growth (15–35% of control) was observed when cells were treated with 10 μM of oxygenated PAHs (PhO, 1,4-chrysenequinone, and 1,8-naphthalic anhydride) and 1 μM of PAQs (phenanthrenequinone and Alz). Most PAHs, however, did not show growth inhibition at the same concentration range (data not shown).

CALUX assay

The CALUX assay was performed using mouse hepatoma (H1L1.1c2) cell lines stably transfected with a luciferase reporter gene under the XREs [16,22]. The range of concentrations in which PACs can be dissolved is shown in a dose–response curve. The value of EC25 for TCDD (15 pM) was four orders of magnitude lower than the EC_{TCDD25} for B[*a*]P (160 nM) (Fig. 3).

The AhR ligand activity of oxygenated PAHs, such as PAKs and PAQs, is shown in Figure 3A–C and in Table 1. Four-ring B[*a*]FO showed significant AhR ligand activity comparable to that of B[*a*]P (EC_{TCDD25} = 450 nM) (Fig. 3B). The potency of four-ring B[*b*]FO (EC_{TCDD25} = 2.3 μM), B[*c*]FO (EC_{TCDD25} = 6.7 μM), NCQ (EC_{TCDD25} = 1.3 μM), 1,4-chrysenequinone (EC_{TCDD25} = 1.9 μM), and BAQ (EC_{TCDD25} = 6.0 μM) also was significant but one order of magnitude lower than that of B[*a*]P (Fig. 3B and C). Five-ring CPPO showed a low activity (EC_{TCDD25} = 43 μM) (Fig. 3B). Most two- and three-ring oxygenated PAHs had either no or very low AhR activities (<25% of maximal activity of TCDD or potency three or more

Table 1. Aryl hydrocarbon receptor (AhR) activation in yeast and mouse hepatoma cell systems and CYP1A1 mRNA induction in HepG2 cells by polycyclic aromatic compounds (PACs) and 2,3,7,8-tetrachlorodibenzo-*p*-dioxin (TCDD)[a]

	Yeast		Mouse		Human			Yeast		Mouse		Human	
Compound	EC_{TCDD25} (nM)	IEF	EC_{TCDD25} (nM)	IEF	EC_{TCDD25} (nM)	IEF	Compound	EC_{TCDD25} (nM)	IEF	EC_{TCDD25} (nM)	IEF	EC_{TCDD25} (nM)	IEF
TCDD	1.3	3.4	0.015	1.1×10^4	0.068	1.9×10^4	Nph	NI		NI			
PhO	2.3×10^3	0.0019	$>6.0 \times 10^4$	<0.0027			ANthyl	U		NI			
BAO	20	0.22	U				ANthe	U		U			
FlO	2.9×10^3	0.0016	NI				Fl	U		NI			
AO	470	0.0096	NI				Ant	U		NI			
XO	990	0.0045	NI				Ph	U		NI			
TXO	280	0.016	U				FA	240	0.019	U			
B[*a*]FO	0.72	6.2	450	0.37			Py	400	0.011	NI			
B[*b*]FO	0.35	13	2.3×10^3	0.072	2.3×10^3	0.58	B[*a*]A	1.1	4.0	640	0.26		
B[*c*]FO	17	0.26	6.7×10^3	0.025			Chr	0.68	6.6	470	0.35		
CPPO	24	0.18	4.3×10^4	0.0038			TPh	49	0.091	U			
BPO	320	0.014	U				B[*b*]F	0.33	14	3.5×10^3	0.046		
AQ	1.4×10^3	0.0032	NI				B[*b*]FA	1.5	3.0	35	4.7		
PhQ	$>1 \times 10^3$	<0.005	U				B[*k*]FA	0.20	22	2.0	84	13	100
ChQ	9.7	0.46	1.9×10^3	0.089			B[*a*]P	4.5	1	160	1	1.3×10^3	1
BAQ	0.28	16	6.0×10^3	0.028			DB[*a,h*]A	15	0.29	18	9.0	200	6.7
NCQ	0.088	51	1.3×10^3	0.13	2.0×10^3	0.66	DB[*a,c*]A	2.2	2.1	180	0.93		
Alz	150	0.030	9.2×10^3	0.018			3-MC	1.2	3.8	310	0.53		
PCQ	NI		U				IdP	4.8	0.93	66	2.5	350	3.8
NA	NI		U				B[*ghi*]Pe	NI		U			
β-NF	0.55	8.1	4.2×10^2	0.39			N[*a*]P	30	0.15	28	5.8		

[a] EC_{TCDD25} = concentration equivalent with 25% of TCDD max. Induction equivalency factor (IEF) is the ratio of EC_{TCDD25} of test compound relative to benzo[*a*]pyrene (B[*a*]P). Data regarding CYP1A1 mRNA induction are from Misaki et al. [25]. PhO = phenalenone; BAO = 7*H*-benz[*de*]anthracen-7-one; FlO = fluorenone; AO = anthrone; XO = xanthone; TXO = thioxanthone; B[*a*]FO = 11*H*-benzo[*a*]fluoren-11-one; B[*b*]FO = 11*H*-benzo[*b*]fluoren-11-one; B[*c*]FO = 7*H*-benzo[*c*]fluoren-7-one; CPPO = cyclopenta[*cd*]pyren-3[4*H*]-one; BPO = 6*H*-benzo[*de*]pyren-6-one; AQ = anthraquinone; PhQ = phenanthrenequinone; ChQ = 1,4-chrysenequinone; BAQ = 7,12-benz[*a*]anthracenequinone; NCQ = 5,12-naphthacenequinone; Alz = alizarin; PCQ = pentacenequinone; NA = 1,8-naphthalic anhydride; β-NF = β-naphthoflavone; Nph = naphthalene; ANthyl = acenaphthylene; ANthe = acenaphthene; Fl = fluorene; Ant = anthracene; Ph = phenanthrene; FA = fluoranthene; Py = pyrene; B[*a*]A = benz[*a*]anthracene; Chr = chrysene; TPh = triphenylene; B[*b*]F = benzo[*b*]fluorene; B[*b*]FA = benzo[*b*]fluoranthene; B[*k*]FA = benzo[*k*]fluoranthene; B[*a*]P = benzo[*a*]pyrene; DB[*a,h*]A = dibenz[*a,h*]anthracene; DB[*a,c*]A = dibenz[*a,c*]anthracene; 3-MC = 3-methylcholanthrene; IdP = indeno[1,2,3-*cd*]pyrene; B[*ghi*]Pe = benzo[*ghi*]perylene; N[*a*]P = naphtho[2,3-*a*]pyrene; U = <25% of TCDD max; NI = not induced.

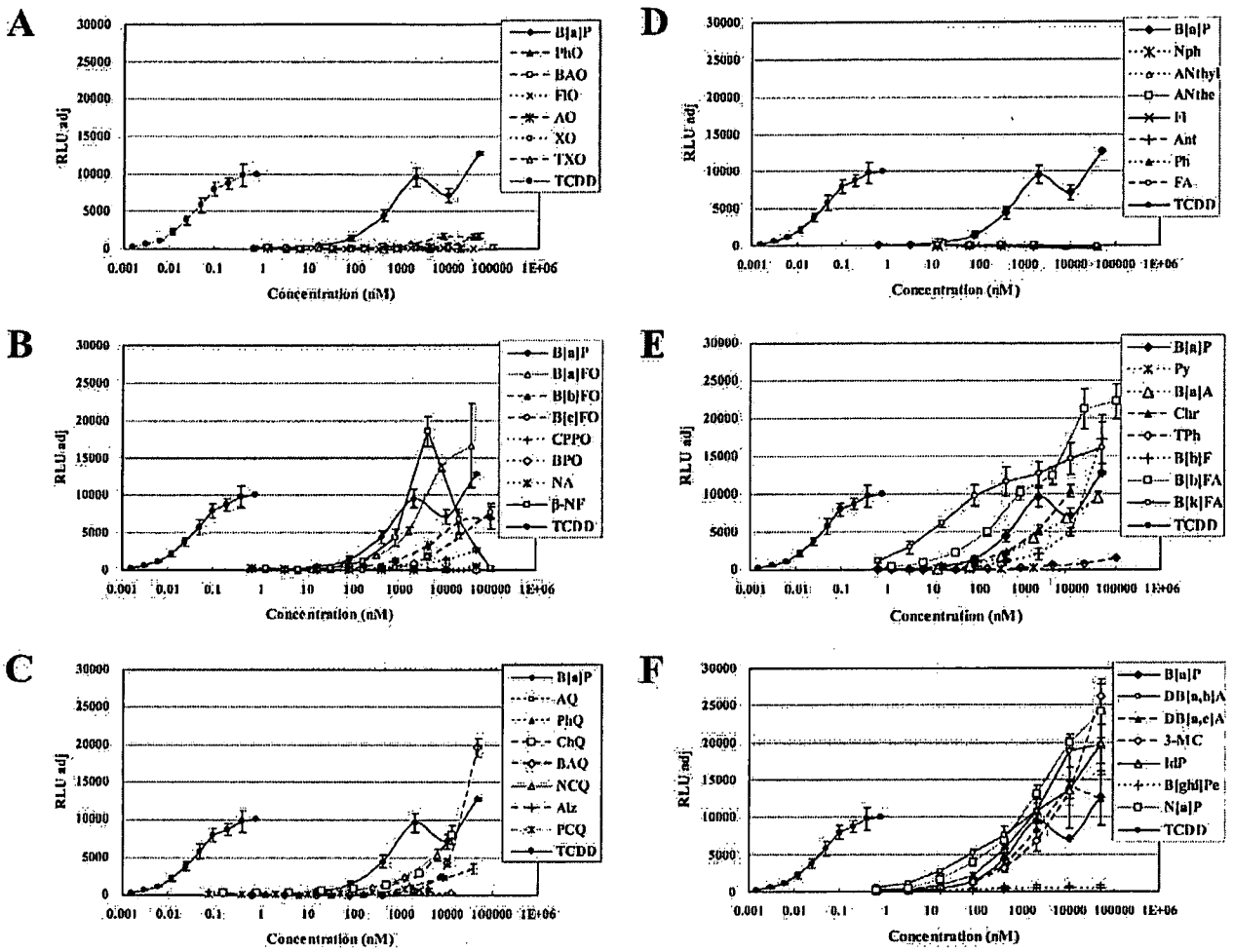

Fig. 3. Luciferase activity in the mouse hepatoma (H1L1) cell system. The H1L1 cells were treated for 24 h with polycyclic aromatic compounds (PACs) and 2,3,7,8-tetrachlorodibenzo-*p*-dioxin (TCDD). See Figure 1 for acronyms of test compounds.

orders of magnitude lower than that of B[*a*]P) (Fig. 3A–C). The potency of Alz was one order of magnitude lower than that of B[*a*]P (EC_{TCDD25} = 9.2 μM) (Fig. 3C). The AhR activities of five-ring oxygenated PAHs, BPO, and PCQ also were less than 25% of maximal activity of TCDD (Fig. 3B and C). Maximal ligand activity of β-NF was shown at 4 μM, but at higher than 4 μM, the induction decreased dependent on concentration (Fig. 3B).

The AhR ligand activity of PAHs also is shown in Figure 3D–F and Table 1. The AhR ligand potency of five-ring B[*k*]FA was strongest among PACs determined in the present study (EC_{TCDD25} = 2.0 nM) (Fig. 3E). Five-ring DB[*a,h*]A (EC_{TCDD25} = 18 nM), B[*b*]FA (EC_{TCDD25} = 35 nM), and IdP (EC_{TCDD25} = 66 nM) and six-ring N[*a*]P (EC_{TCDD25} = 28 nM) also showed relatively strong potency (Fig. 3E and F). Four-ring Chr (EC_{TCDD25} = 470 nM), B[*a*]A (EC_{TCDD25} = 640 nM), and B[*b*]F (EC_{TCDD25} = 3.5 μM) were slightly weaker AhR agonists than B[*a*]P (Fig. 3E). All two- and three-ring PAHs had either no or very low AhR activities (<25% of maximal activity of TCDD) (Fig. 3D). Four-ring FA, pyrene and triphenylene, also had either no or very low AhR activities (luciferase activity was observed for FA at ~200 μM) (Fig. 3D and E). The AhR activity of six-ring B[*ghi*]Pe was less than 25% of maximal activity of TCDD (Fig. 3F). It was characteristic that AhR activation by B[*a*]P decreased, but then increased between 2 and 50 μM (an N-type curve).

The exfoliation of H1L1 cell from culture plate was observed when cells were treated with 100 μM of some PAKs, such as PhO, BAO, FlO, anthrone, and B[*a*]FO, and 10 μM of phenanthrenequinone for 24 h. All PAHs, however, did not show the significant exfoliation at the concentration where PAHs can be dissolved.

DISCUSSION

Comparison of yeast assay and CALUX assay

AhR activation by oxygenated PAHs and PAHs. In the CALUX assay in mouse hepatoma (H1L1) cells, TCDD was at least three orders of magnitude (1,000-fold) more potent than the PAHs as an AhR ligand, whereas its potency in β-galactosidase assay in yeast cells was similar to that of several PAHs (Table 1). The ratios of the EC_{TCDD25} in yeast assay to the EC_{TCDD25} in CALUX assay for oxygenated PAHs (PAKs and PAQs) were lower than the ratios for most PAHs. It also was observed that the ratios of the EC_{TCDD25} in yeast to the EC_{TCDD25} in H1L1 cells for low-ring-number PAHs having AhR ligand activity were lower than the ratios for high-ring-number

Table 2. The ratios of the concentration equivalent with 25% of maximal response to 2,3,7,8-tetrachlorodibenzo-*p*-dioxin (TCDD) (EC_{TCDD25}) in yeast cell system to the EC_{TCDD25} in mouse hepatoma cell system by polycyclic aromatic compounds (PACs) and TCDD and their hydrophobicities

Compound	Ratio of EC_{TCDD25}	Log K_{OW}
TCDD	87	6.80[a]
Oxygenated PAHs		
11*H*-Benzo[*a*]fluoren-11-one	1.6×10^{-3}	4.79
11*H*-Benzo[*b*]fluoren-11-one	1.5×10^{-4}	4.47
7*H*-Benzo[*c*]fluoren-7-one	2.5×10^{-3}	4.53
Cyclopenta[*cd*]pyren-3[4*H*]-one	5.6×10^{-4}	4.53
1,4-Chrysenequinone	5.1×10^{-3}	4.89
7,12-Benz[*a*]anthracenequinone	4.7×10^{-5}	5.29
5,12-Naphthacenequinone	6.8×10^{-5}	5.05
Alizarin	1.6×10^{-2}	3.48
β-Naphthoflavone	1.3×10^{-3}	4.50
Nonoxygenated PAHs		
Benz[*a*]anthracene	1.7×10^{-3}	5.79[b]
Chrysene	1.4×10^{-3}	5.73[b]
Benzo[*b*]fluorene	9.4×10^{-5}	5.77[b]
Benzo[*b*]fluoranthene	4.3×10^{-2}	5.97
Benzo[*k*]fluoranthene	0.10	6.07
Benzo[*a*]pyrene	2.8×10^{-2}	5.97[b]
Dibenz[*a,h*]anthracene	0.83	6.50[b]
Dibenz[*a,c*]anthracene	1.2×10^{-2}	6.17[b]
3-Methylcholanthrene	3.9×10^{-3}	6.91
Indeno[1,2,3-*cd*]pyrene	7.3×10^{-2}	6.71
Naphtho[2,3-*a*]pyrene	1.1	7.49

[a] Shiu et al. [31].
[b] Smith and Hansch [32].

PAHs as AhR ligands (e.g., B[*a*]A and Chr vs B[*b*]FA, B[*k*]FA, B[*a*]P, and so on) (Table 2).

Speed of uptake. The speed of uptake of chemicals by the cells would tend to create a bias that, potentially, would underestimate the potency of hydrophobic compounds relative to that of hydrophilic compounds in yeast cells (PAHs are more hydrophilic than TCDD, PAKs and PAQs are more hydrophilic than PAHs, and low-ring-number PAHs are more hydrophilic than high-ring-number PAHs). The speed of uptake of chemicals may be influenced by factors as follows [14]: 1) Low pH, low protein, and low lipid content of yeast media in comparison to typical mammalian tissue culture media have a poor capacity to bind and transport hydrophobic compounds; and 2) the thick yeast cell wall constitutes a diffusion barrier for hydrophobic compounds, whereas hydrophobic compounds permeate cell membrane of mammalian cells easily. In fact, a significant correlation was found between the ratio of the EC_{TCDD25} in yeast cell system to the EC_{TCDD25} in mouse hepatoma cell system for chemicals and the K_{OW} values of them ($p < 0.006$), and the linearity of this correlation was weak ($R = 0.59$) (Fig. 4 and Table 2).

Speed of metabolism. The speed of metabolism of these compounds would be the second possible factor in underestimating the potency of TCDD relative to that of PAHs in yeast cells. It was suggested that resistance to metabolism appeared to be a key determinant of TCDD's biological potency and toxicity via AhR from the comparison study of biological potency, such as CYP1A1 induction by TCDD and one PAH, 3-MC, in mouse hepatoma cells [15]. Each compound did not differ dramatically in the ability to activate processes in the CYP1A1 induction mechanism that occurred after initial binding to the AhR (TCDD and 3-MC differed in affinity/potency

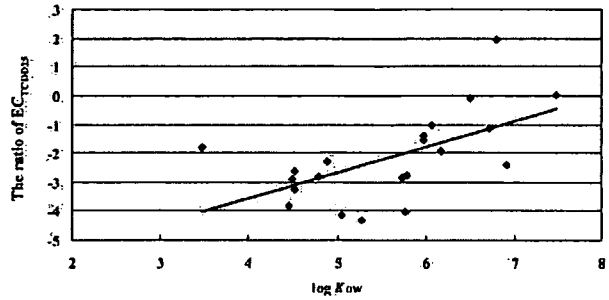

Fig. 4. Correlation between the ratios of the concentration producing galactosidase activity equal to 25% of the maximal response to 2,3,7,8-tetrachlorodibenzo-*p*-dioxin (TCDD) (EC_{TCDD25}) in yeast cell system to the EC_{TCDD25} in mouse hepatoma cell system by chemicals and their hydrophobicities ($y = 0.8963x - 7.1576$; $r = 0.59$, $p < 0.006$, $n = 21$). The p value was determined by t test.

by, at most, only fourfold in vitro, and these differed in potency by 4- to 25-fold in nuclear translocator of AhR, CYP1A1 mRNA induction at 2 h, and AHH induction at 4 h). However, the greater rate of metabolism of 3-MC appeared to limit its biological potency in intact cells (TCDD was 100- to 1,000-fold more potent than 3-MC for AHH induction at 14 h and CYP1A1 mRNA and chloramphenicol acetyltransferase induction at 16 h) [15]. It was demonstrated that EROD activity by endogenous CYP enzyme in yeast microsomes ranged from 6- to 400-fold less than the EROD activity observed with human liver microsomes [34]. Therefore, it was predicted that metabolization of every AhR ligand active compound in the present study is more difficult in yeast cells than in mammalian cells [15,34]. In the present study, several low-ring-number PAHs (FA, pyrene, triphenylene, and so on) and several low-ring-number oxygenated PAHs (BAO, anthrone, xanthone, and so on) showed potencies from one to three orders of magnitude lower than that of B[*a*]P in yeast cells, whereas their activities were either zero or less than 25% of maximal activity of TCDD in mouse hepatoma cells. This also possibly was derived from the metabolic speed of them in yeast cells being lower than in mammalian cells. It may be that oxygenated PAHs are metabolized more rapidly than PAHs and that low-ring-number PAHs are metabolized more rapidly than high-ring-number PAHs. The reports about comparison for metabolic speed of various PACs by several enzymes in mammalian cells, however, are few.

Conformation of AhR and AhR regulators. Lower AhR potency of TCDD in yeast cells than mammalian cells also may be caused by the reduction of ligand-binding activity in the polymorphic form of human AhR [19,35]. In fact, human AhR is less sensitive to TCDD than C57BL/6 mouse AhR [19,35]. Therefore, a yeast cell line transfected with a mouse AhR gene likely would yield potency estimates for AhR ligands that are more similar to those of the other mammalian cell bioassays than those generated using a yeast cell line transfected with human AhR [36]. Additionally, the difference of AhR regulators (e.g., chaperones such as XAP2, heat-shock protein 90, and p23) may contribute to the difference of AhR activity between yeast and mammalian cells [14,37].

CALUX assay. In the CALUX assay, mouse hepatoma (H1L1.1c2) cell line stably transfected with a luciferase reporter gene under the XREs is used [22,38]. Ziccardi et al. [16] showed that 1 nM TCDD and 100 nM B[*a*]P caused maximum induction at 4 and 3 h, respectively, then declined

Table 3. The contribution of each polycyclic aromatic compound (PAC) to aryl hydrocarbon receptor (AhR) activity in gasoline exhaust particulates by using the chemical-activated luciferase expression (CALUX) assay

Compound	IEF[a]	Emission level[b] (μg/km)	IEQ[c]	Contribution of each PAC[d]
Anthracene	NI[e]	0.7		
Phenanthrene	NI	2.6		
Fluoranthene	U[f]	20		
Pyrene	NI	28		
Benz[*a*]anthracene	0.26	5.7	1.5	0.80%
Chrysene	0.35	6.7	2.3	1.2%
Benzo[*b*]fluorene	0.046	26[g]	1.2	0.64%
Benzo[*b*]fluoranthene	4.7	3.9[h]	9.2	4.9%
Benzo[*k*]fluoranthene	84	3.9[h]	164	88%
Benzo[*a*]pyrene	1	1.9	1.9	1.0%
Indeno[1,2,3-*cd*]pyrene	2.5	1.7	4.3	2.3%
Benzo[*ghi*]perylene	U	5.9		
Phenalenone	<0.0027	15	0.041	0.022%
7*H*-Benz[*cd*]anthracen-7-one	U	3.4		
Fluorenone	NI	7.4		
Xanthone	NI	15		
11*H*-Benzo[*a*]fluoren-11-one	0.37	6.6	2.4	1.3%
11*H*-Benzo[*b*]fluoren-11-one	0.072	6.8	0.49	0.26%
7*H*-Benzo[*c*]fluoren-7-one	0.025	2.8	0.070	0.037%
6*H*-Benzo[*cd*]pyren-6-one	U	3.5		

[a] Induction equivalency factor (IEF) relative to benzo[*a*]pyrene (mouse hepatoma cell system).
[b] Induction equivalent (IEQ) relative to benzo[*a*]pyrene (emission level multiplied by IEF).
[c] Saab 900 GL with a 2-L, four-cylinder, noncatalyst gasoline engine (data from Alsberg et al. [3]).
[d] Percentage IEQ in the sum of calculated IEQs.
[e] NI = not induced.
[f] U = less than 25% of the maximum response to 2,3,7,8-tetrachlorodibenzo-*p*-dioxin (TCDD).
[g] Including benzo[*a*]fluorene. The IEQ is calculated by assuming that this value as the total amount of benzo[*b*]fluorene.
[h] This value is the sum of benzo[*b*]fluoranthene and benzo[*k*]fluoranthene. The IEQs for these PACs are calculated by assuming that half this value is the total amount of each compound.

in these cells, and those authors suggested that this decline may be related to cell type–specific instability of the luciferase protein and/or an effect resulting from elements at the specific site of genomic integration of the plasmid In fact, Han et al. [39] developed another mouse hepatoma (H1L6.1c2) cell line in which induction by TCDD increased until 24 h. Also, B[*a*]P caused significantly greater induction at 6 h than at 24 h, whereas induction by TCDD increased until 24 h in reporter gene assays conducted by several researchers using rat and human hepatoma cells [6,12,17,38]. The CALUX assay at 24 h reflects the metabolism of PACs and seems to be appropriate for the evaluation of long-exposure toxicity, such as endocrine-disrupting activity of PACs via the AhR pathway except for the effect on a fetus, the metabolic capabilities of which are reduced. The rank-order potency of induction for PACs at 24 h in reporter gene assay using H1L1.1c2 cells was similar to that in other mammalian cells, such as rat and human hepatoma cell lines, but time-dependent induction change by TCDD was different between them [6,12,16,17,39].

Induction of CYP1A1 mRNA. In our previous study, the IEF value of CYP1A1 mRNA amount in human hepatoma (HepG2) cells exposed to six representative PACs and TCDD was examined (Table 1) [25]. No exclusive difference was found between the IEF value of CYP1A1 mRNA amount in HepG2 cells and that of this CALUX assay in H1L1 cells. The CYP1A1 mRNA inductions by 5 μM PAHs (B[*a*]P, B[*k*]FA, DB[*ah*]A, and IdP) and 5 μM oxygenated PAHs (NCQ and B[*b*]FO) in HepG2 cells did not decrease even if exposure was continued for 72 h [25]. The AhR activity of NCQ and B[*b*]FO relative to B[*a*]P in HepG2 cells (IEF = 0.66 and 0.58, respectively) was somewhat higher than that in the CALUX assay (IEF = 0.13 and 0.072, respectively) (Table 1), and this may be related to the difference of stability of mRNA or protein of CYP1A1 and luciferase depending on species, cell lines, or detection methods [6,12,38]. The relationship, however, was not clear.

Chemical structure and AhR conformation. The AhR protein conformation and ligand-binding pocket have not been determined, but the size of the pocket was predicted from AhR ligand molecular structure. From other studies on AhR binding affinity, it was predicted that classical AhR active compounds were planar and had maximum dimensions of 14 × 12 × 5 Å, but some new class ligands do not necessarily fit to this size [19,22,35,40]. In the present research about reporter gene assays of PACs, potent AhR ligands, such as B[*b*]FA, B[*k*]FA, B[*a*]P, DB[*a,h*]A, IdP, and N[*a*]P, and, to some extent, highly active AhR PAHs, such as B[*a*]A, Chr, and B[*b*]F, and oxygenated PAHs, such as B[*a*]FO, B[*b*]FO, BAQ, and NCQ, fit for this size (Fig. 1 and Table 1). Low AhR active ligands, such as FA, pyrene, and BAO, however, were slightly smaller in size, and two- and three-ring, small-size PACs and big-size PACs, such as B[*ghi*]Pe and PCQ, showed either no or very low AhR ligand activity. High-affinity binding is thought to also result from electrostatic interactions of the ligands with AhR [19,22,40]. This may be supported by the fact AhR-binding activity of Alz is, to some extent, high, whereas that of anthraquinone is either low or zero. Further study is needed for examining the effect of electrostatic interactions by substituents of oxygenated PAHs on AhR binding affinity.